Spray Heat Transfer Research at CINVESTAV

Sami Vapalahti,* Humberto Castillejos E, F** Andrés Acosta G,** Alberto C. Hernández B, A.** and Brian G. Thomas***

***Laboratory of Metallurgy,**
Helsinki University of Technology, Finland

****Laboratory of Process Metallurgy,**
CINVESTAV, Mexico

*****Department of Mechanical Science & Engineering,**
University of Illinois at Urbana-Champaign

1 Transient Experiments

In transient measurements a plate of steel is heated in a furnace to a desired temperature and then quickly moved from the furnace in to a holder. Before the measurement is made the desired flow conditions are adjusted. There is a wooden panel in front of the sample holder so the spray can be kept on while the sample is placed into it. The sample is a rectangular plate and a picture of a sample unassembled and assembled in Fig. 1 ready for thermocouples respectively.

Fig. I. Sample unassembled and ready for the thermocouples and experiment.

Figs. 2, 3 and 4 illustrate how the measurement is made. The wooden plate used for blocking the spray before the hot plate is in place can be seen Fig. 5.

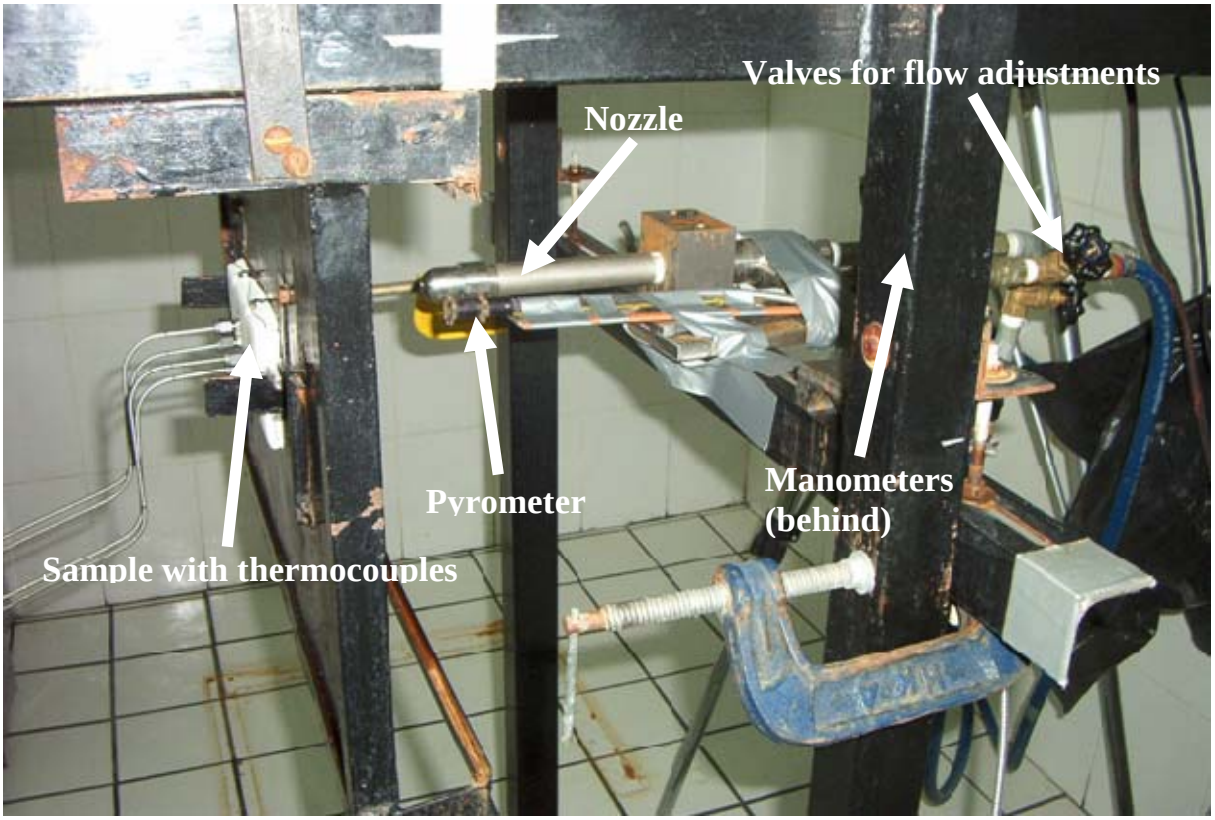

Fig. 2. The sample has to be adjusted in place before setting into the furnace.

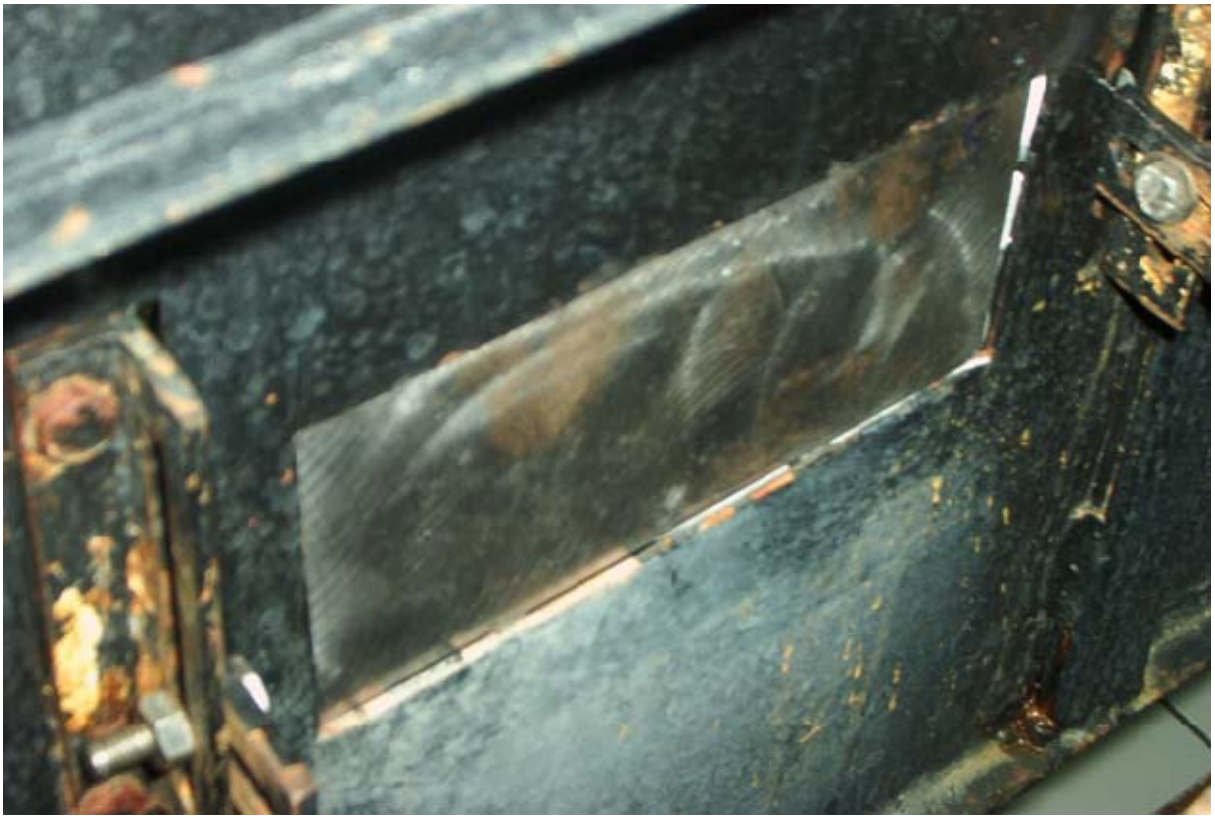

Fig. 3. Sample as exposed to the spray.

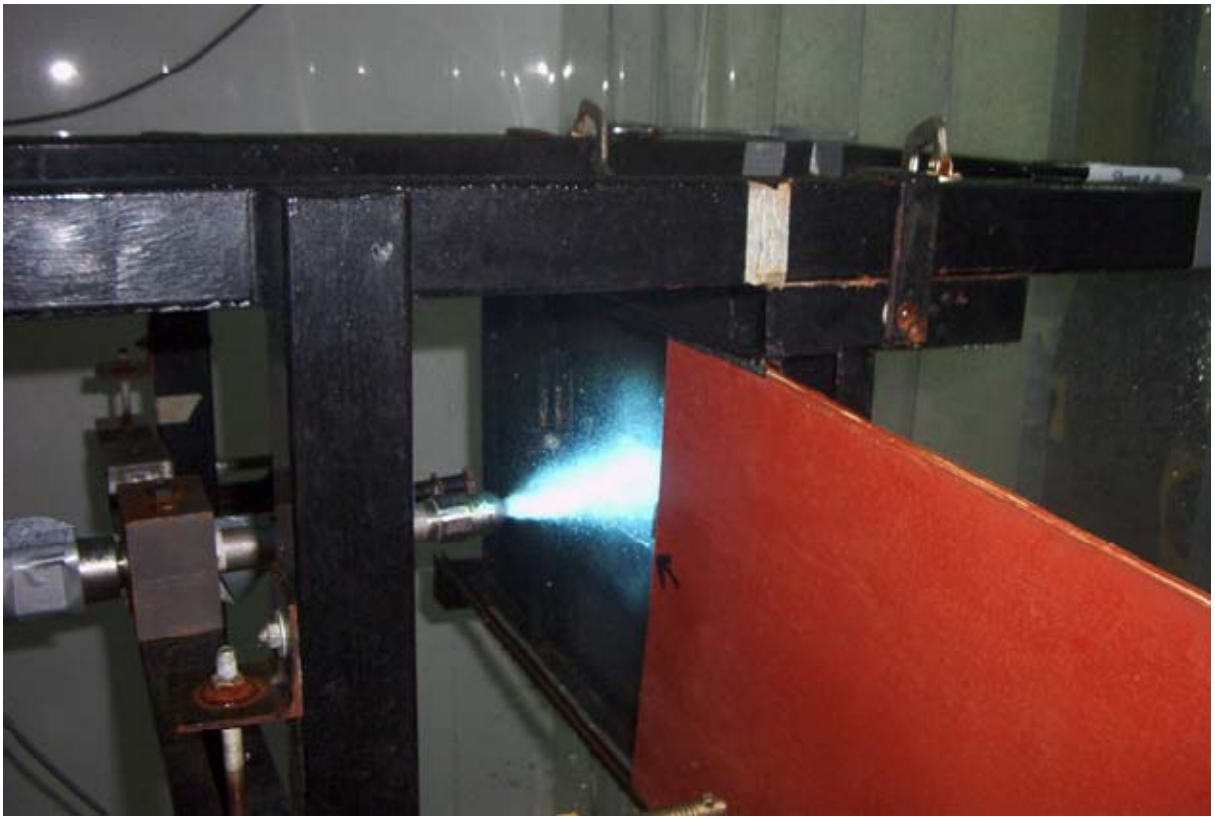

Fig. 4. The wooden plate has been drawn aside and spray hits the sample.

After the measurement is over the pressures, water temperature, and dislocation of the sample in the holder are recorded. The DAQ-system on the computer records flow rates and temperatures.

1.1 Analysis of The Results

The cooling curves measured in the experiments need to be converted into heat flux at the surface and the surface temperature has to be calculated. This is done using an inverse model CONTA. Inverse heat conduction problem (IHCP) is an “ill-posed” problem and does not satisfy general conditions of existence, uniqueness and stability causing a difficulty in defining what the solution is. This means that for every realistic surface flux history, temperatures can be calculated as a function of time at an interior position. Other values arbitrarily close to these calculated temperatures can be produced with an infinite number of surface fluxes. Each of these fluxes would have the same basic heat flux as the original case but there could be high frequency sinusoidal components superimposed upon the basic heat flux. Because of that it is required to restrict the surface flux to having acceptable time variations.

Many methods to solve IHCP have been proposed but most of them can only solve linear cases. The most widely used method to solve nonlinear case is a sequential and involves the use of future temperatures for each calculated component of the surface flux. By sequential is meant estimating one or some small number of components of heat flux at each time step instead of trying to iterate the whole set of heat flux components at once. This procedure permits much smaller time steps than making calculated interior temperatures equal the measured values and allows much more information to be derived about time variation of the surface heat flux than large time steps.

As the time steps are made small, the oscillations tend to have higher amplitudes and frequencies. High frequency in IHCP context means flux components with periods equal or shorter as the time steps between the heat flux components. These high frequencies then need to be filtered out to stabilize the solutions. There are many ways for doing that but in CONTA the function specification method is used meaning the surface heat flux is given a functional form. Function is created using number of constants derived from measured temperatures by least square method.

To increase computational speed of CONTA some simplifications are made that may affect the accuracy of the results.

- The first is assumption of materials properties from previous time step in present and in the selected amount of future time steps. This is done in order to avoid iteration and give the equation a linear form.
- A temporary assumption of constant heat flux over the future time steps used in finding the heat flux of the present time.

In the case of this study with cooling rates over 200°C/s these simplifications has to be taken into account when the time step size is selected. [1]

1.2 Sensitivity Analysis of The Inverse Model

Plate 5 thermocouple 1 in the second experiment was selected as the test case for this investigation. There are three parameters in the inverse code that need to be investigated: time step between data points, number of future time steps and time step of the calculation.

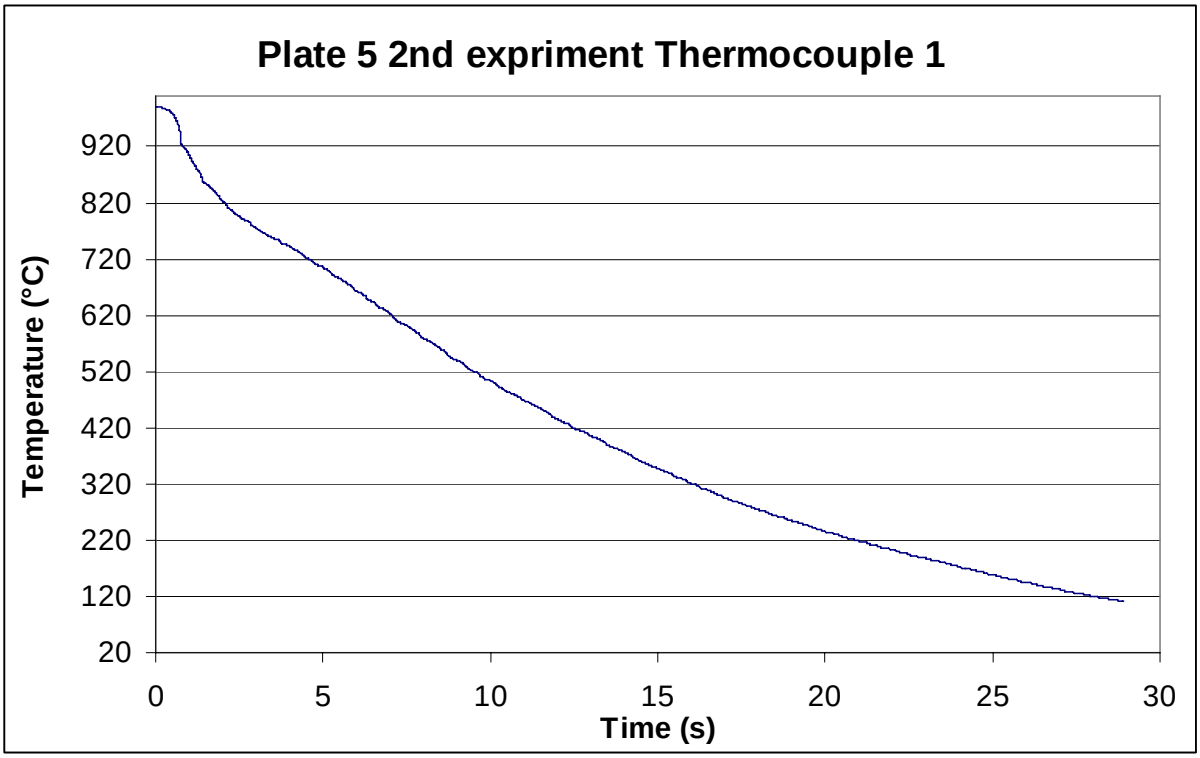

Figure XX. Cooling curve for the analyzed thermocouple data.

1.2.1 Sensitivity of The Measured Data

The first objective was to determine if there is a need to artificially expand the collected data or is the amount of data points sufficient for the inverse model. For this purpose the data for the test case was expanded by inserting certain amount of data points linearly distributed between original measurement points. Cases with 1, 4, 7, 9 and 14 inserted points were calculated. In Fig. 1 it is possible to see that peak heat flux increases with the amount of data points until at 14 inserted values the calculation becomes unstable. This instability is due to mathematical nature of the inverse model and would require the amount of future time steps to be changed for stability. This, as shown later, would again increase the error in heat flux.

Interestingly accuracy at low temperatures becomes worse but this is due to calculation time step as shown in Fig. 8. In Fig. 2 the results zoomed on high temperatures.

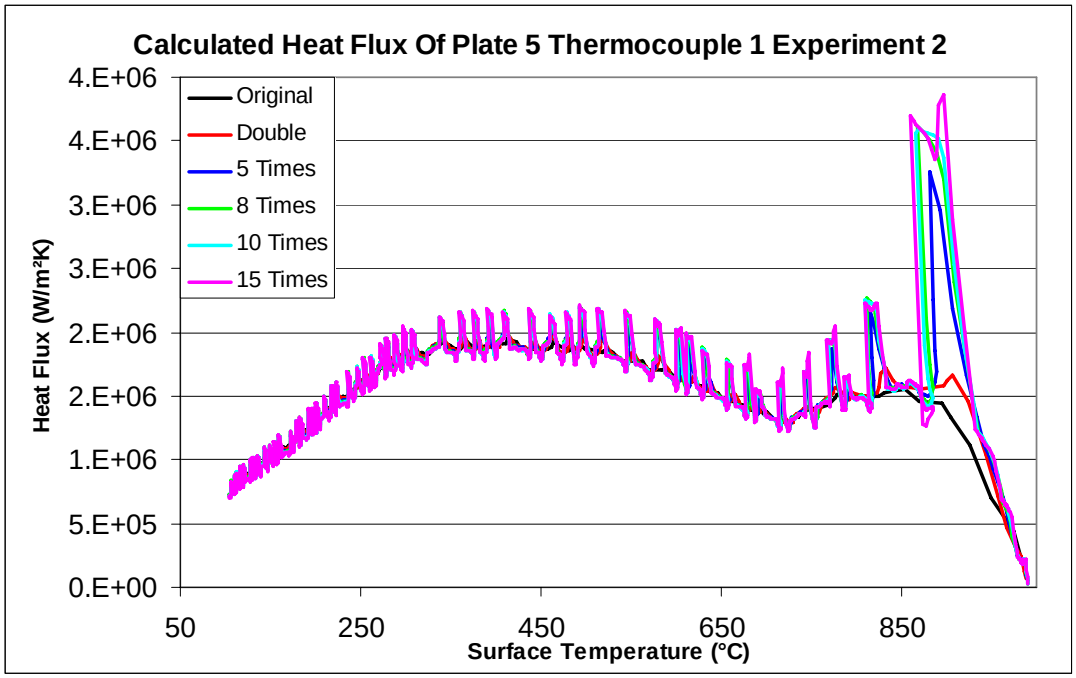

Fig.1. Original and 2, 5, 8, 10, and 15 times more data points effect on heat flux.

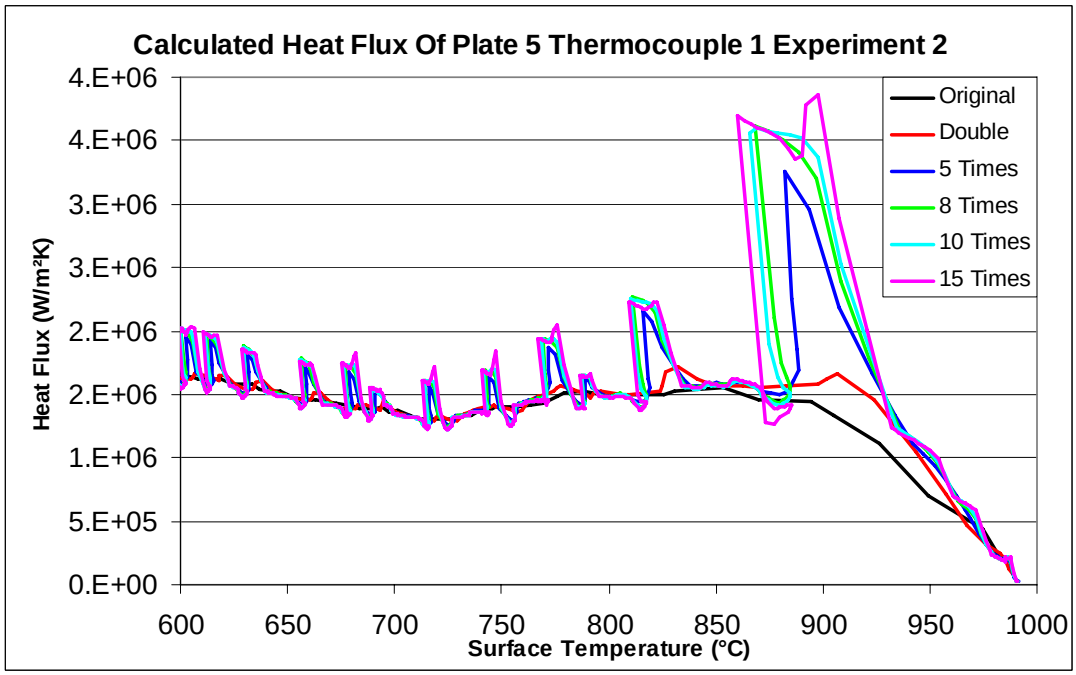

Fig. 2. Results zoomed at high temperatures.

When the amount of data points increases the error between measured and calculated temperatures decreases. In low temperatures, as shown in Fig. 3, the error increases and the maximum accuracy is reached using twice the amount of points compared to original data. Again this is due to too large calculation time step.

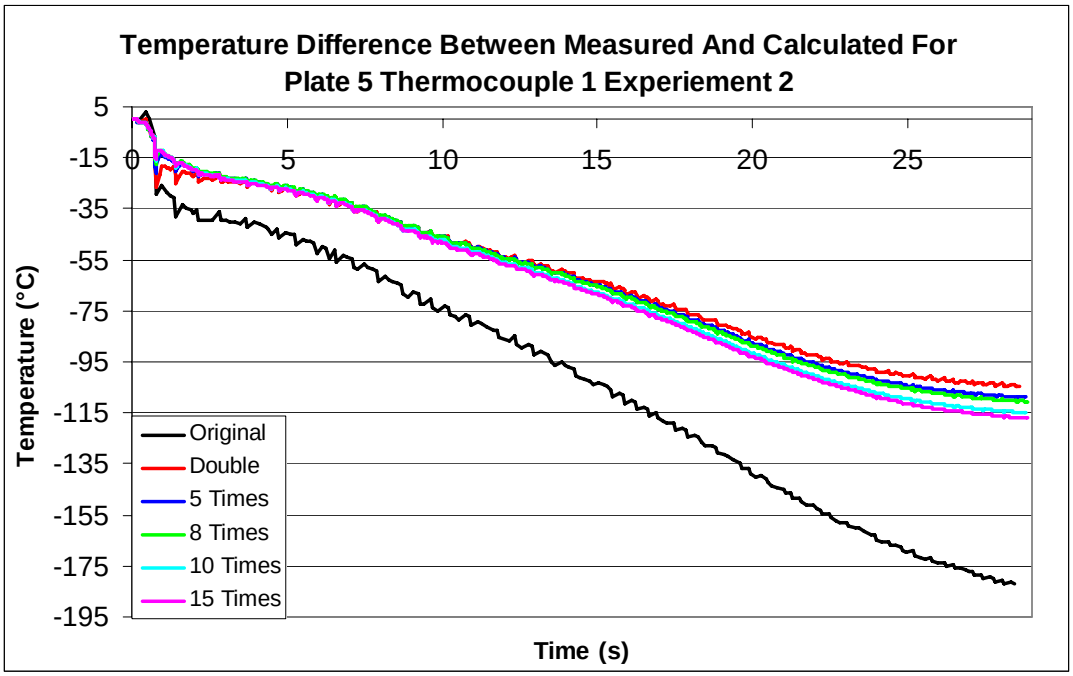

Fig. 3. Error between measured and calculated temperature.

In Fig. 4 the results are only shown for the first 7.5 seconds where the main focus is. It can be seen that nine inserted points gives the best result.

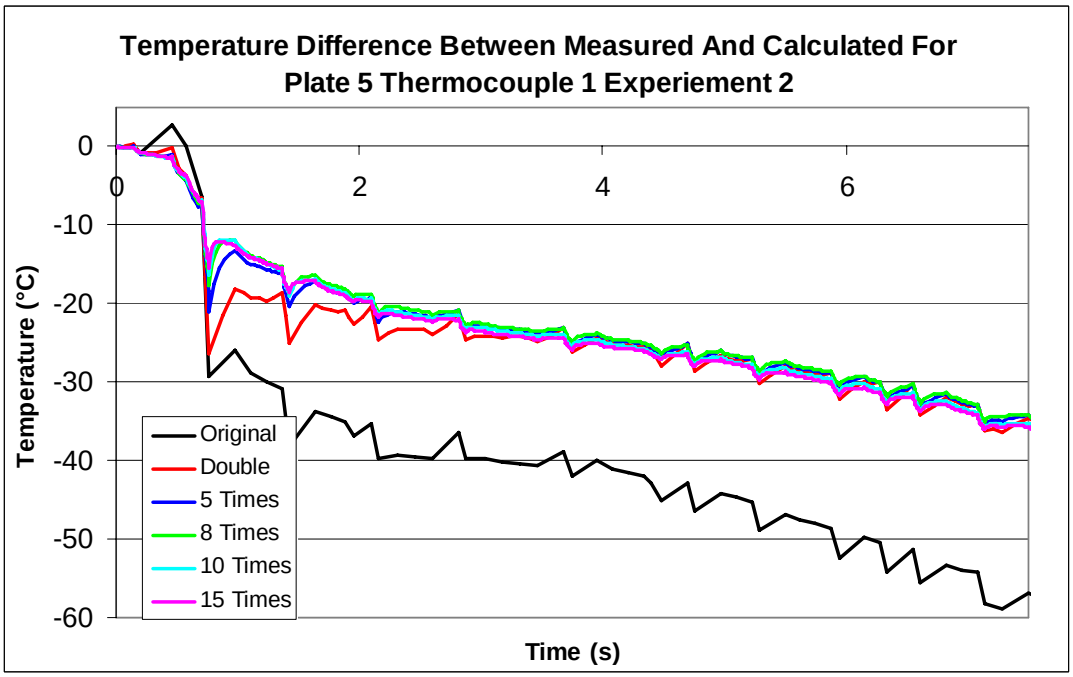

Fig. 4. The error between measured and calculated temperatures at high temperatures for original amount, 2, 5, 8, 10, and 15 times more data points.

1.2.2 Sensitivity of The Future Time Steps

According to previous results, to insert 9 linearly distributed data points between original measurement data, gives the best inverse analysis possible with used inverse model. The next step is to investigate how many measured points in the future should be taken into account when the inverse analysis is made. This has to be done in order to minimize oscillation of the solution. This oscillation can be already seen in the results and the instability it causes when the time scale of

these future time step is too small compared to analyzed data. In Fig. 5 it can clearly be seen that in investigated case four future time steps gives the best results.

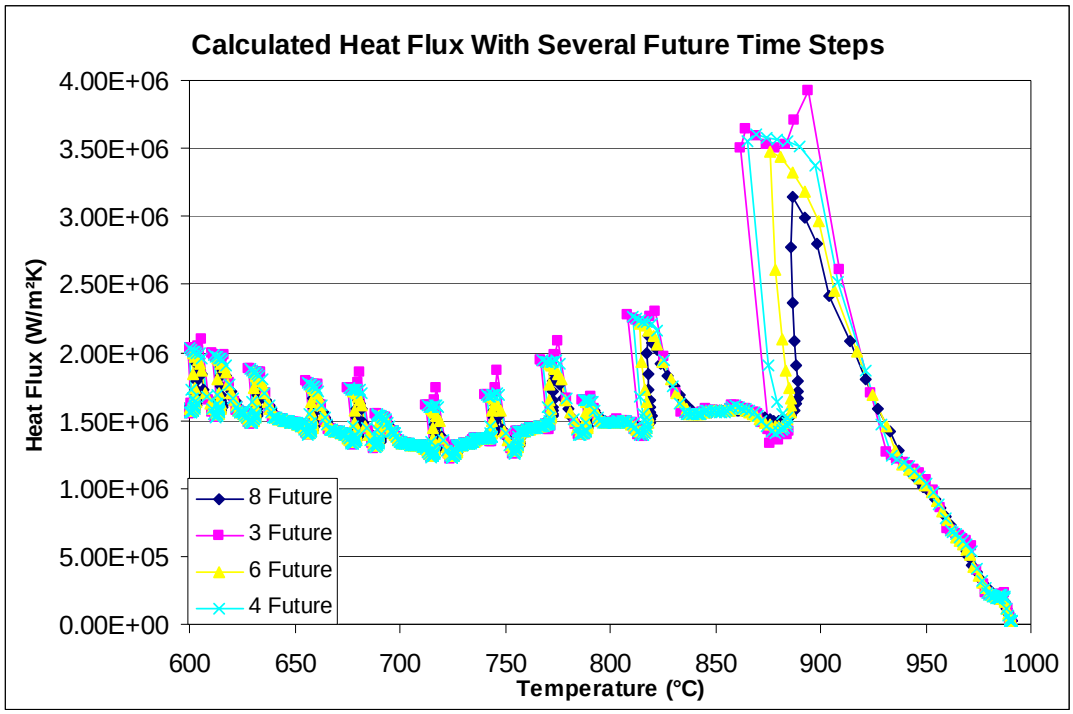

Fig. 5. Heat flux as a function of surface temperature for several future time step parameters.

1.2.3 Sensitivity of The Calculation Time Step

The last parameter to be investigated is the calculation time step. Based on previous results nine inserted data points and four future time steps were selected as the test case. Time steps 0.001, 0.0005, 0.0001, and 0.00005 are used in simulations. In Fig. 6 it is possible to see that 0.0001 is sufficient time step for these calculations.

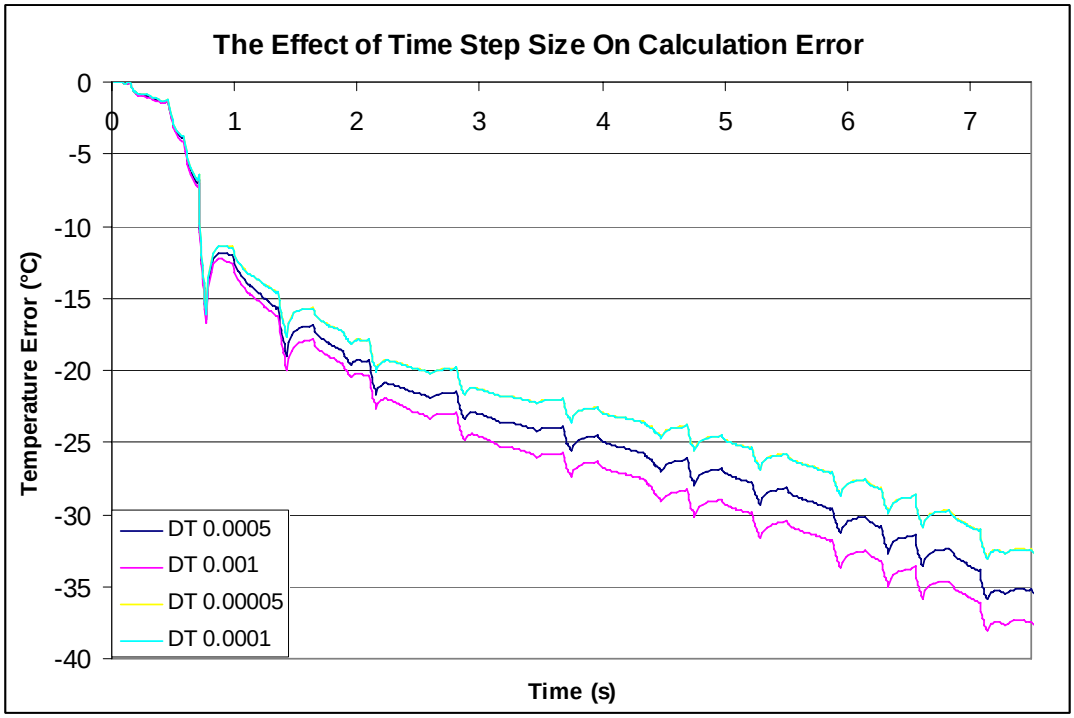

Fig. 6. Error between measured and calculated temperatures for several time step size.

Time steps 0.0001 and 0.00005 give the same results making 0.00005 invisible.

1.2.4 Differences Between Original And Manipulated Data Calculations

In Fig. 7 heat flux profiles for manipulated and original data cases is presented. The biggest difference occurs during nine first measurement points meaning during 0.45 seconds. It shows how fast the data acquisition should be in order to capture the cooling curve accurately with high performance air-mist nozzles. Cooling rate in this particular case is small compared to 100-300°C/s recorded for some measurements.

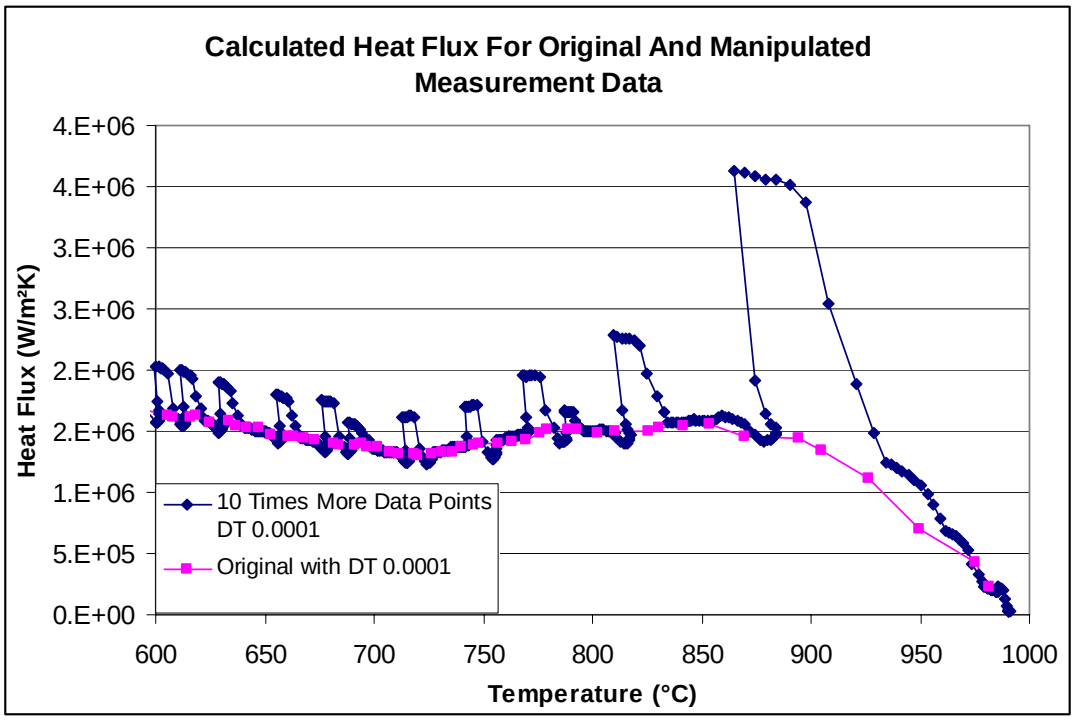

Fig. 7. Heat flux profiles for original and manipulated data.

In Figs. 8 and 9 the error between calculated and measures temperatures is presented. It still is a question why this error keeps increasing at lower temperatures but as the range of interest is at temperatures over 600°C it is not feasible to try to correct it.

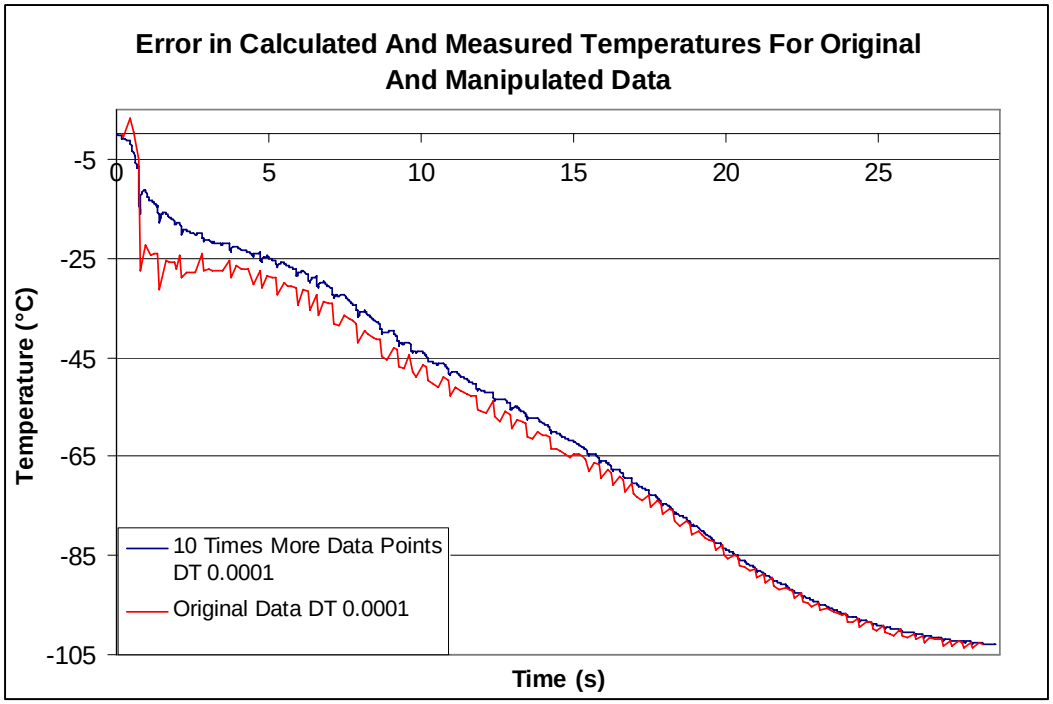

Fig. 8. Calculation error compared to measured temperature for original and manipulated data case.

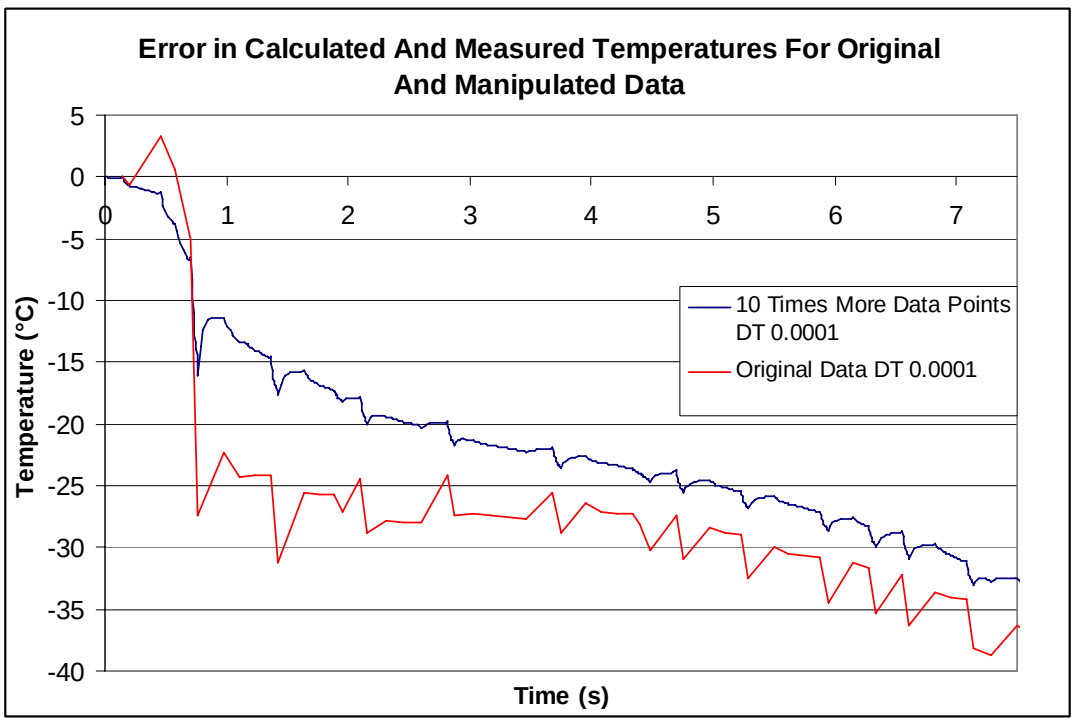

Fig. 9. Error on the range of interest at temperatures over 600°C.

1.2.5 Conclusion

Some improvement can be made in inverse analysis if data is manipulated but the truth is that if data acquisition is not fast enough this data is lost and calculations become inaccurate. But it seems, at least for the case in question, that the error is at acceptable level even with the original data. Data manipulation is probably more feasible with higher cooling rates where future time steps cut heat flux even more. Also it has to be taken into account that thermocouples have a response time that will affect the crucial first moments of the experiments where the heat flux, especially in the case of

air-mist sprays, are extremely high. This will cause some error to the peak heat flux values. These aspects need to be taken into account when the results of the transient experiments are evaluated and compared to steady state experiments.

2 Steady State Experiments

This report describes a new experimental system to measure heat flux during spray cooling based on steady-state conditions, along with preliminary results. This was done to augment and improve on previous measurements, which have been based on transient conditions. During transient conditions, heat transfer changes both with time (development of boundary layers of water and steam) and with temperature (as the substrate surface temperature drops). The steady-state experiments described here aim to find the true steady-state heat transfer after the boundary layers have developed.

The first step to find steady state heat extraction rates for various spray nozzles at different temperatures and under various spraying conditions, an induction-based heating equipment was purchased and the measurement technique developed. Next, heat fluxes were extracted from the results using a combination of measurements and modelling. Finally, the new measurements are compared with previous transient measurements for the same conditions. This work aims to investigate the importance of transient heat transfer phenomena in spray cooling and to find the time scales of these phenomena in the surface-temperature range 300-1200°C. This temperature range includes all spray cooling done for steels e.g. during continuous casting and rolling.

2.1 Equipment

In the Fig. 1 the setup is described in detail.

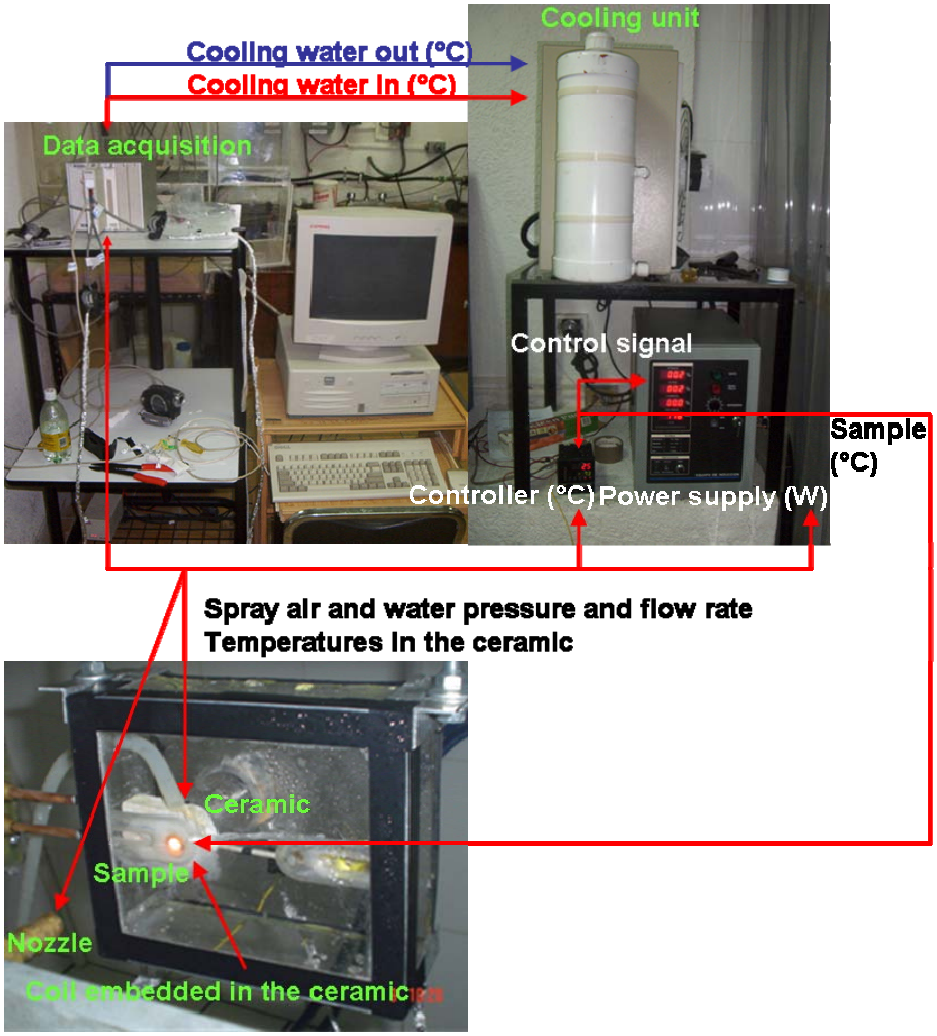

Figure 1. Steady state spray cooling apparatus.

Using National Instruments SCXI-1000 box together with two SCXI-1302 terminals several signals are collected from the measurement system: sample temperature from the controller, total power taken by the power supply, cooling water temperature raise between the cooling unit and power supply, two surface temperatures from the ceramic and spray properties including pressure and flow rates for both air and water. Acquisition sampling time is 0.05 seconds. All cables are shielded either by manufacturer using a braid and that has been grounded or simply applying aluminium foil around the cables as done in the case of thermocouples. The nominal maximum power the power supply can deliver is 5000W but it can be loaded up to 110% of the nominal making the maximum to be 5500W. Thermocouples used are of K-type. Currently also water temperature measurements are made using exposed tip K-type thermocouples. Samples used are AISI-304L stainless steel that is paramagnetic in order to avoid problems caused by the Curie-temperature and to minimize oxidation. The materials properties of the ceramic, steel and copper are given in the Appendix A.

A schematic shape of the sample is shown in the Fig. 2. The thermocouple used for controlling the temperature in the sample is welded in the centre, the closest place to the sprayed surface and the heating is applied on the periphery of the sample where induction currents circle the sample surface within the skin depth. The skin depth, δ, is the thickness of the superficial layer where the induced current is practically confined and it is defined using Eq. 1.

$$\delta = \frac{1}{\sqrt{\pi f \mu \sigma}} = \sqrt{\frac{\rho}{\pi f \sigma}} \qquad (1)$$

Where π is 3.1416, f is the electromagnetic frequency (Hz), μ and σ are the magnetic permeability (H/m) and the electric conductance (1/(Ωm)) of the metal, and ρ resistivity (Ωm) of the metal, respectively. It the case of AISI 304L with the frequency of the current coil the skin depth is:

Magnetic Permeability	1.2629E-06	Weber
Resistivity	7.20E-07	Ohmm
Frequency	2.92E+05	Hz
Skin depth	0.78833702	mm

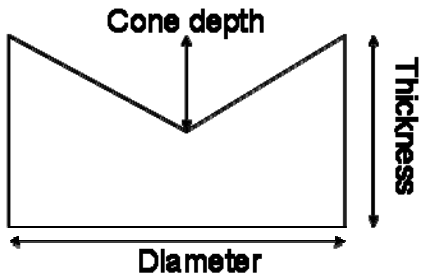

Figure 2. Schematic picture of a sample. Descriptions and parameters for all produced samples are in the Appendix A in the Table 1.

The sample is inserted into the coil embedded in ceramic to minimize heat losses and to protect the sample from any water touching the lateral or back side of the sample. The coil dimensions and the shape are shown in the Fig. 3.

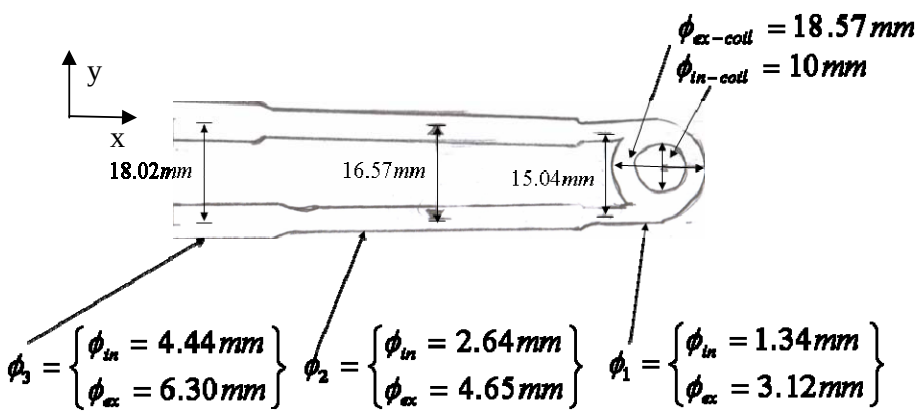

Figure 3. Copper coil top view. It consists of one and a half turns with one millimetre of air between the turns. Water flows into the coil from the upper left copper tube and exits lower left.

The sample location in respect of the coil is shown in the Figs. 4 and 5.

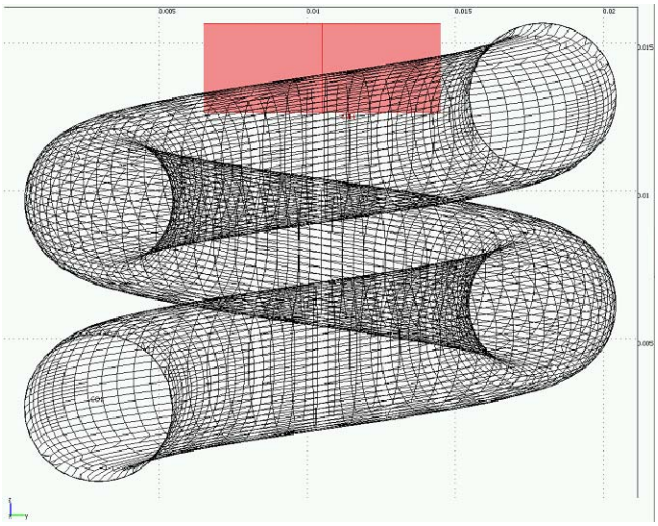

Figure 4. The coil and the sample on Y-Z-plane (end view) Water enters the upper right hole and exits lower left.

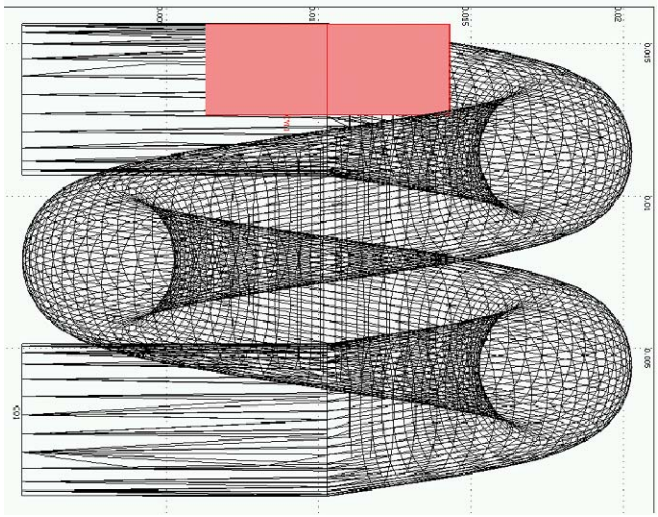

Figure 5. The coil and the sample on X-Z-plane (side view).

The dimensions of the coil together with the ceramic are illustrated in Figs. 6, 7, 8, and 9. These figures also so the locations of the thermocouples that were used for measuring the ceramic surface temperature during the experiments in order to estimate the heat losses from the sample to other directions that the front surface. These thermocouples were located in the lateral side and the back side of the ceramic and are named TC1 and TC2 respectively.

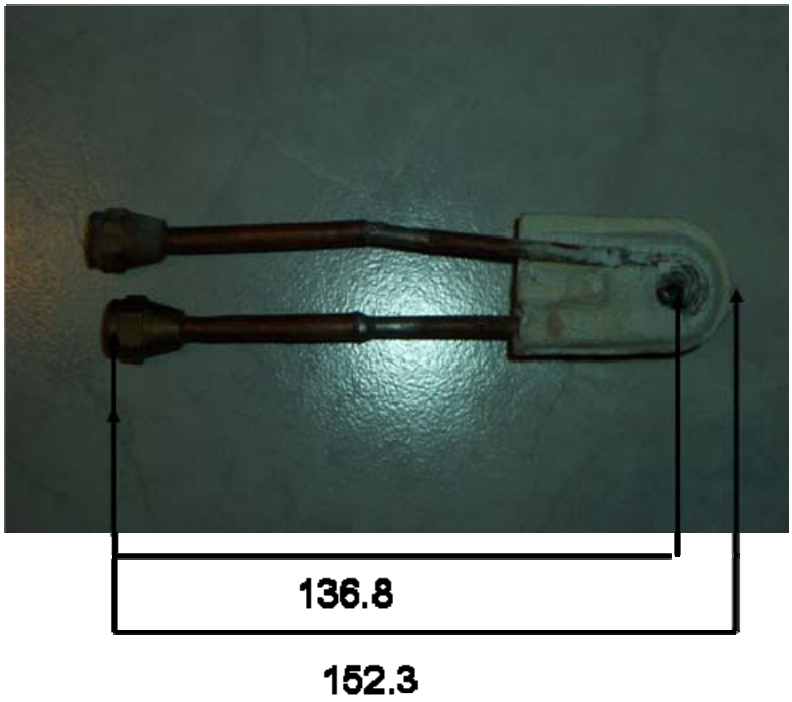

Figure 6. Coil dimensions with the ceramic.

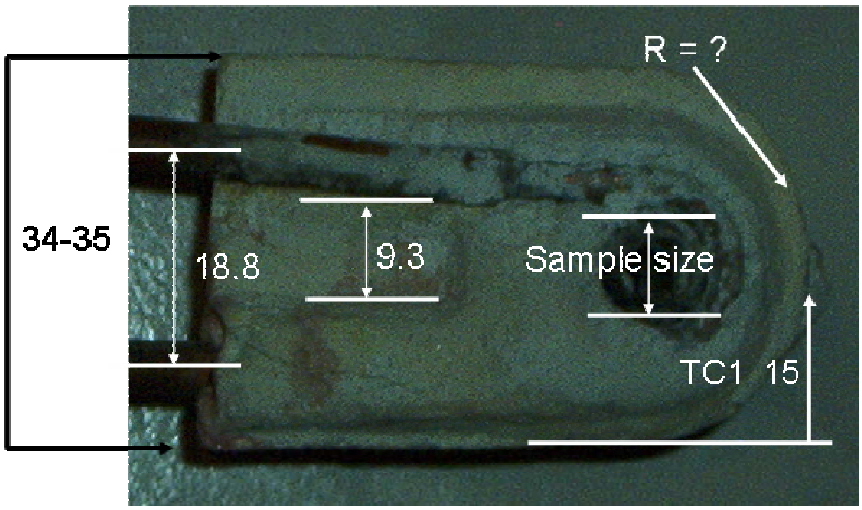

Figure 7. Dimensions of the ceramic and TC1 Y-coordinate.

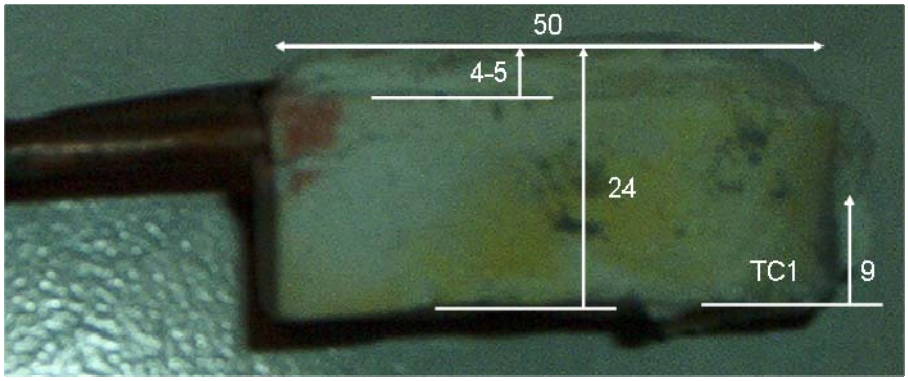

Figure 8. Dimensions of the ceramic and TC1 Z-coordinate.

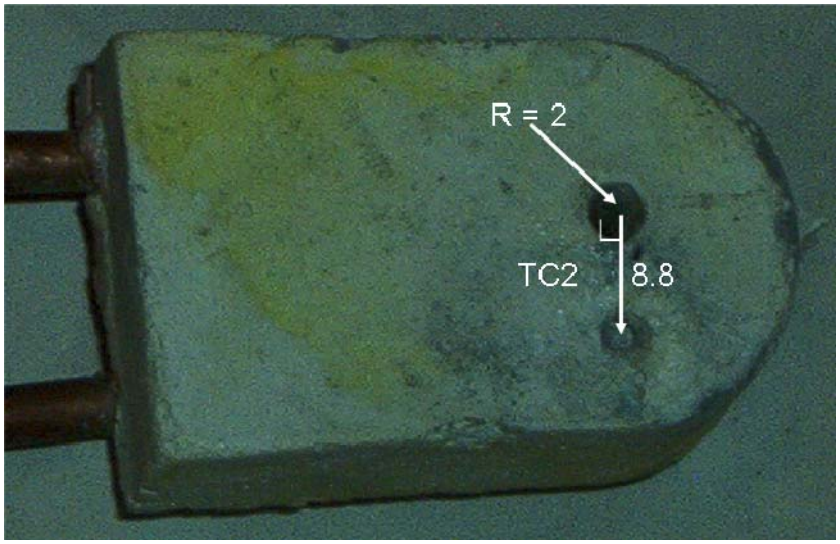

Figure 9. Dimensions of the ceramic and the location of the TC2.

The shape of the front surface of the ceramic was obtained by casting the wet ceramic on to the carved shape on the quartz window used for protecting the sample from getting exposed to water from other sides that the front surface. The dimensions of the quartz glass are shown in the Fig. 10.

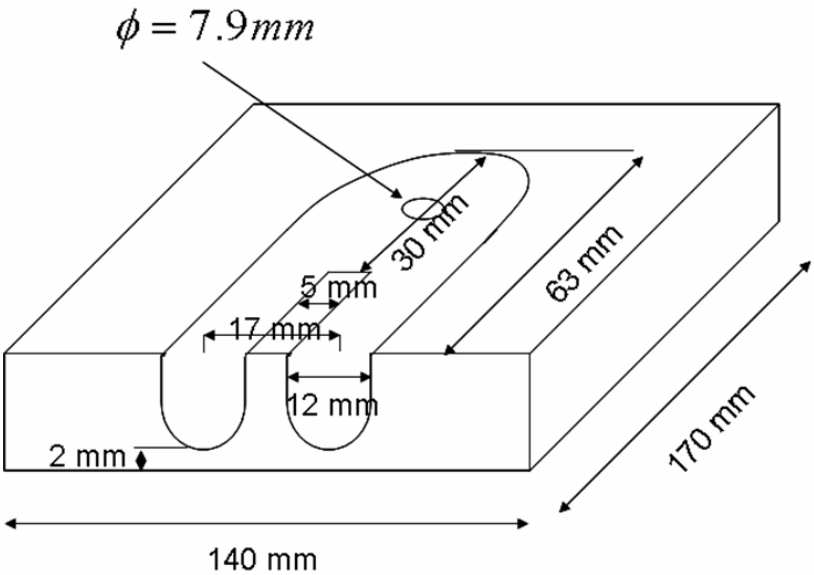

Figure 10. Quartz glass dimensions. The coil and the sample are cast into ceramic (Fig. 6, 7, 8, and 9) and pressed against the glass as shown in Fig. 1 to prevent any water intrusion to other faces of the sample.

2.2 Power Measurements and Efficiency

Total power distribution is presented in Fig. 11. P_{tot} is the measured total power used by the power supply. This power includes the power lost to the cooling water, the power used to heat up the motor with time, and the power lost to ambient air, in addition to the power delivered to the sample.

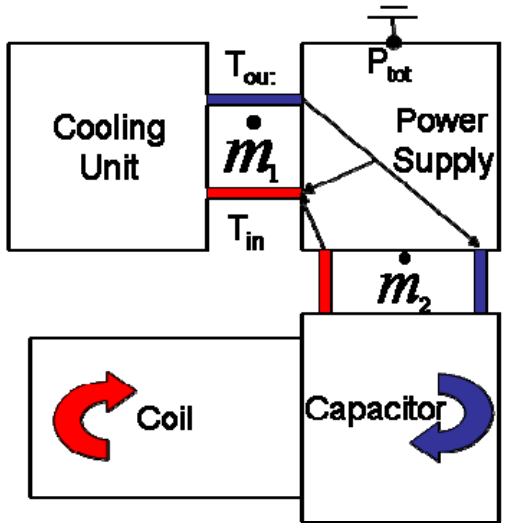

Figure 11. Schematic presentation of the induction apparatus and the measured quantities.

In the induction apparatus a part of the power, P_{ps}, is lost during running the equipment that cannot be directly measured. This power is not entering the cooling water but is lost in to the air and to heat up the equipment. It is assumed that this power loss is unique to the induction system consisting of a power supply, cooling unit, capacitor and a particular coil. It is further assumed that this power loss in not affected by the fact weather there is a sample inside the coil, called a load, or not. This means that changes in heat loss to the air (which increases as the motor heats up) matches the change in heat absorbed into the system (which decreases as steady-state is approached) P_{ps} is possible to measure if the apparatus is run without a load and at the same time the part of the power, P_w, which is entering the cooling water, is measured. Then P_{ps} is:

$$P_{ps} = P_{tot} - P_w \tag{2}$$

As can be seen in Fig. 11, after the cooling water leaves the cooling unit and enters the power supply, the cooling water is divided into two mass flows. One flow stream circulation is made within the power supply and the other circulation goes through a capacitor and then through the coil connected to the sample. To find P_w, the mass flow $\dot{m}_1$, T_{in}, and T_{out} have to be measured

$$P_w = C_p \dot{m}_1 (T_{in} - T_{out}) \tag{3}$$

Where C_p is water specific heat, $\dot{m}_1$ water mass flow, T_{in} temperature of the cooling water coming in to the cooling system after circulation, and T_{out} temperature of the cooling water leaving the cooling system to cool the system. C_p is selected to be constant water specific heat at 30°C 4179 J/kgK. During the experiments the water temperature was not allowed to heat above 41°C. Due to excess heating of the power supply while running without any load, the maximum power was limited to 45% (2250W) of the nominal power and most of the measured points concentrate on lower power values. In Fig. 12 P_{ps} from the measurements are plotted as a function of the total power. The regression line is forced to go through (0,0) since there can be no lost power if there is no total power.

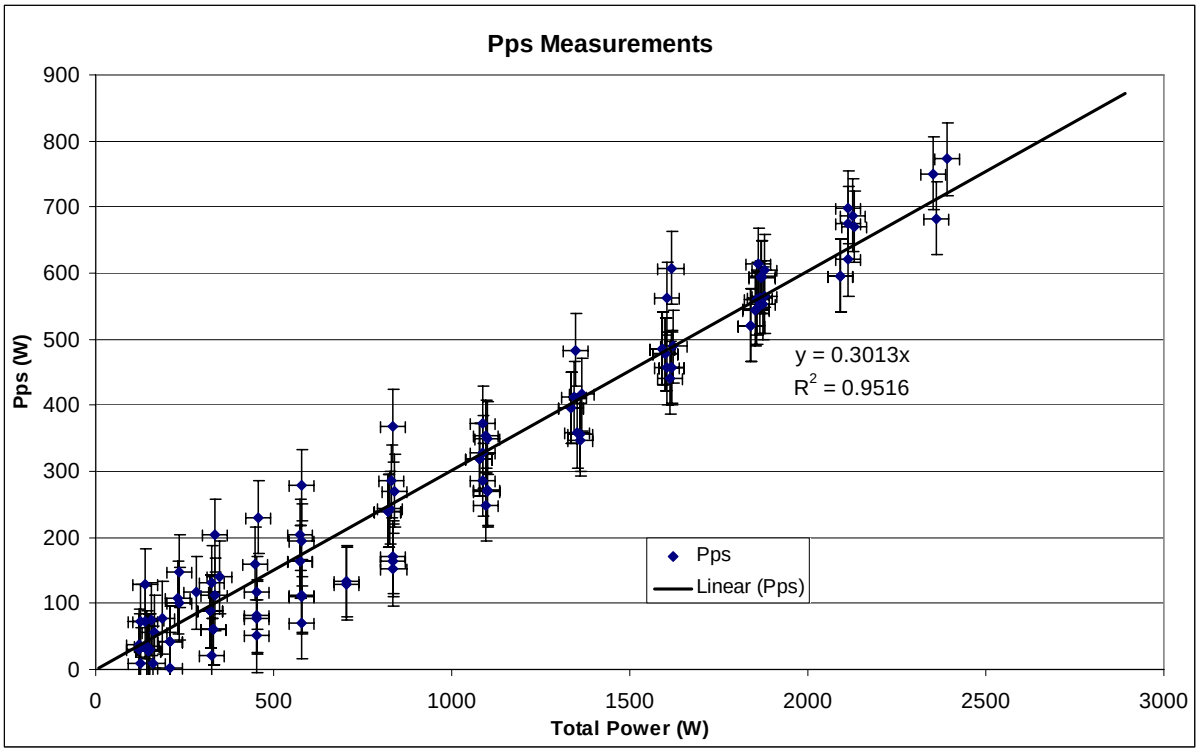

Figure 12. Measured P_{ps} as a function of the total power.

It was found out that P_{ps} is a linear function of the total power with some uncertainty.

$$P_{ps} = (1-\eta_{ps}) \times P_{tot}, \tag{4a}$$

The power supply efficiency, η_{ps}, is seen to be ~70%, based on the slope of 0.3013 in the figure.

The known Y-error is caused by inaccuracy of the total power and cooling water measurements (±35W and ±20W respectively) and X-error caused by inaccuracy in total power measurement. The experiments using the samples were made with the measurement setup corresponding to the P_{ps} measurement in the Fig. 12. The total power of all measurements were multiplied with a coefficient named Potencia actual derived from the Fig. 12. Actual power can be calculated using Eq. 4b.

$$P_A = \eta_{ps} \times P_{tot} \tag{4b}$$

Where P_A is the measurable power used for heating the sample and cooling water of the whole induction apparatus, P_{tot} the total measured power from the power supply.

As the high level of scattering was noticed the cabling was altered in order to lower the amount of the scattering. In Fig.13 the P_{ps} measurements for the new cabling are shown and noticeable change in the slope can be seen. As can be seen the scattering is greater than error caused by known measurement errors in both cases. Causes for the error can be behaviour of the equipment changes when water cooling unit is on or the power supply's internal temperature change. The known measurement errors are caused by noise in the measurement system. Noise in total power measurement has now been decreased to ±1.5W. Noise in cooling water power still remains the same and we expect some improvement by replacing the thermocouples and possibly rewiring.

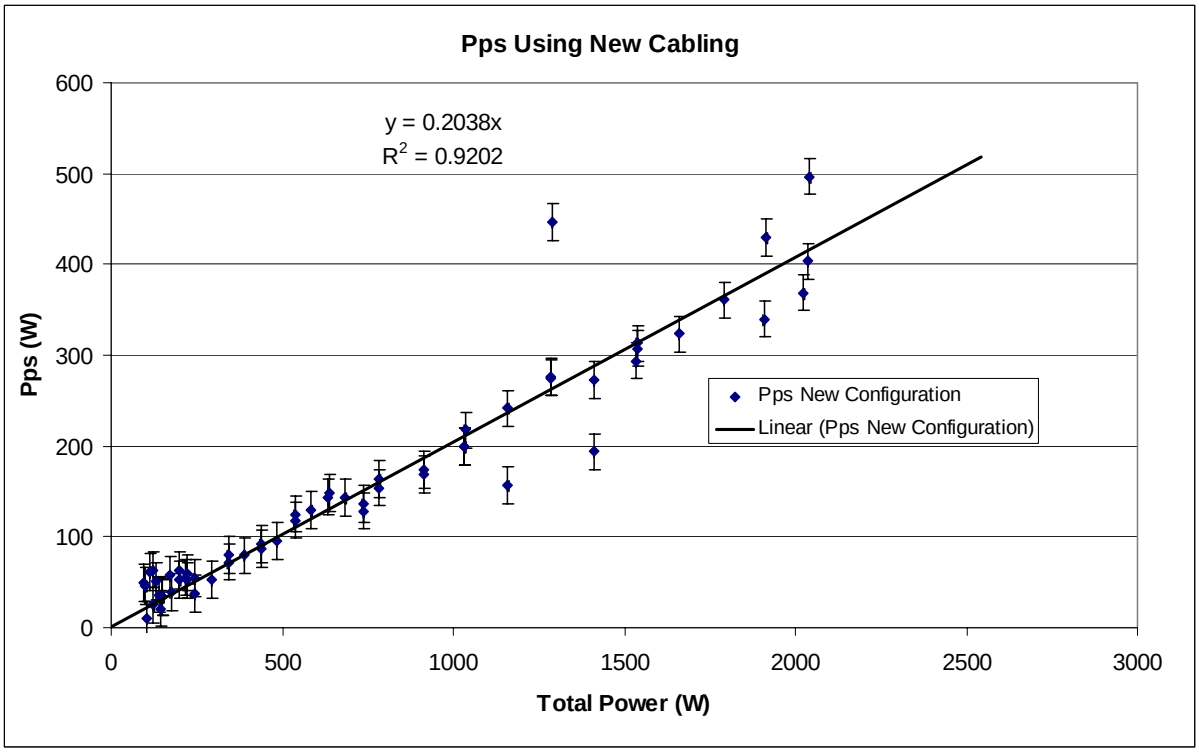

Figure 13. Measurement results of the P_{ps} with new cabling.

Efficiency increased to ~80% after making this change. Thus, efficiency η_{ps} should be remeasured for each experiment in the future where changes have been made in the measurement system.

After getting P_A, the next step is to find the efficiency η_{is}, which will indicate the fraction of the measurable power P_A that is actually used for heating up the sample. To find η_{is} the sample is heated up in ambient air to the temperatures planned to be target temperatures during the spray experiment. In this ambient air experiment, heat input to the sample is split into estimated heat losses to the lateral, the back side, and the front of the sample. η_{is} is referred in the spread sheet results files as Eficiencia (prom).

$$\eta_{is} = \frac{\left(P_{front} + P_{annular} + P_{back} + P_{lateral}\right)}{P_A} \times 100 \tag{5}$$

In ambient air cooling the total power, sample temperature, and the two ceramic temperatures were recorded. Unfortunately, the temperature measurement in the cooling water was not yet available. The heat losses to ambient in the case of the ceramic were calculated using simple Fourier's' law:

$$P_{lateral\ ,back} = -k\left(\frac{T_{sample} - T_{TC\,1,2}}{dx_{TC\,1,TC\,2}}\right) * A_{Lateral\ ,back} \tag{6}$$

Where k the conductivity of the ceramic, T_{sample} is the sample temperature, T_{TC1} the lateral, T_{TC2} the back surface thermocouple measurement, and dx the distance from the sample surface to the thermocouple. $A_{lateral}$ is the lateral area of the sample calculated for each sample using the Table 1 in Appendix A with Eq. 7. In the result files lateral area is named Area 2 and P_2 is the lateral and P_3 the back surface heat loss respectively

$$A_{lateral} = \pi dh \tag{7}$$

Where π constant, d is sample diameter and h is sample thickness. A_{back} is called Area 3 and is calculated by neglecting the conicity of the back surface using Eq. 8:

$$A_{back} = \frac{\pi d^2}{4} \tag{8}$$

The lateral thermocouple (TC1) distance dx_{TC1} is shown in the analyzed excel files under name distancia p2. It includes an assumption that the distance shown in Figs. 7 and 8 can be neglected because the coil acts as a cooling channel between the thermocouple and the sample. The actual distance dx_{TC1} is then the distance from the sample surface to the surface of the coil and the thermocouple reading is assumed to be valid at that location. The back face thermocouple (TC2) distance dx_{TC2} has been treated as is given in the Figs. 8 and 9 and is shown in the files under name distancia p3.

The heat loss through the front surface is calculated using radiation as shown in Eq. 9:

$$P_{front,annular} = \sigma\varepsilon\left(T_{sample}^4 - T_{amb}^4\right) \times A_{front,annular} \tag{9}$$

Where σ is Stefan-Boltzmann constant, ε is the emissivity of steel, T_{sample} sample temperature and T_{amb} the ambient temperature. In the result files P_{cont} is referred as P_1, A_{front} as A_{1a}, $A_{annular}$ as A_{1b}, and T_{amb} as T_a. A_{front} can be calculated from Eq. 10 and $A_{annular}$ from Eq. 11 using constants Diametro a and sample diameter. These are illustrated better in the Fig.14.

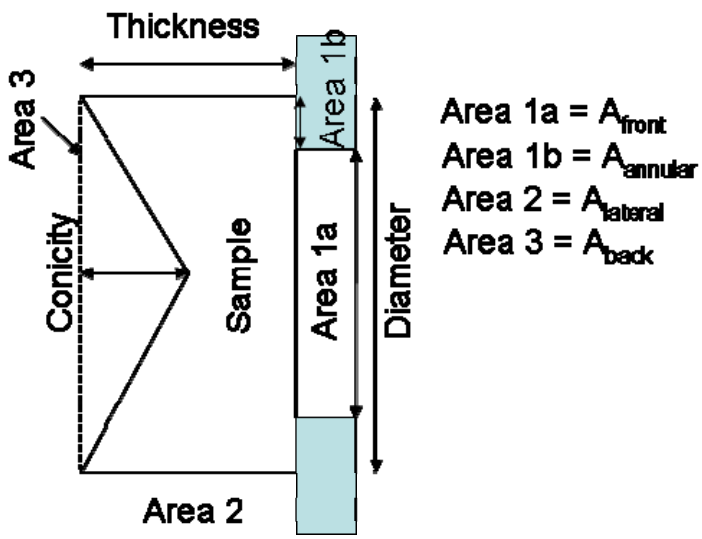

Figure 14. Schematic presentation of the sample attached to the quartz glass.

$$A_{front} = \frac{\pi\left(Diameter\right)^2}{4} \tag{10}$$

$$A_{annular} = \frac{\pi}{4}\left(d^2 - \left(Diameter\right)^2\right) \tag{11}$$

Where Diametro a is given in the results file and sample diameter d in the Appendix A Table 1. Temperatures are averages over the time the sample was kept on a target temperature, usually 20 seconds.

2.3 Results

Depending on how well the sample is conserved during the experiments without melting or strong oxidation, only one or two thermal cycle experiments can be made when using a stainless steel sample. In this case sample 36 was used. First the ambient air cooling experiment was conducted in order to find out the efficiency of the induction heating. In Table 1 the necessary constants to conduct calculations mentioned in the chapter 1.2 are shown.

Table 1. Constants for calculating the efficiencies for sample 36.

Constantes		
σ =	5.67E-08	
ε =	0.8	Unidades
Ta =	298	K
Diametro a =	0.0061	m
Espesor anular	0.000905	m
Espesor =	0.00335	m
Conicidad =	0.00059	m
Π =	3.1416	
Area 1a =	2.9225E-05	m2
Area 1b =	1.9916E-05	
Area 2 =	6.4199E-05	m2
Area 3 =	4.9141E-05	m2
k =	0.57639	W/mK
ρ =	1762.031	Kg/m3
cp =	740	J/kg K
α =	4.4205E-07	m2/s
distancia p2 =	0.0015	m
distancia p3=	0.01939	m
tiempo	20	s
potencia actual =	0.6987	

In the Tables 2, the averaged measured quantities are shown together with calculated power losses through front, lateral and back faces and the efficiency calculation for sample 36.

Table 2. Calculated heat losses, actual power and efficiency for each target temperature for sample 36.

Temperatura	P1a	P1b	P2	P3	Pa (prom)	Eficiencia Prom
1200	6.23026445	4.24583899	28.3811652	1.66245156	466.962985	8.677287392
1100	4.7004662	3.20330266	25.9804422	1.52240222	405.954319	8.721822043
1000	3.470812	2.36531034	23.5933012	1.38145044	355.712639	8.661731586
900	2.49921032	1.70317724	21.2274051	1.23979759	304.616965	8.755123098
800	1.74675114	1.19038672	18.9014168	1.09755486	257.610996	8.903389169
700	1.17770598	0.80259032	16.5239162	0.95502204	217.005942	8.967143637
600	0.75952788	0.51760774	14.1054871	0.8122408	183.845872	8.808935096

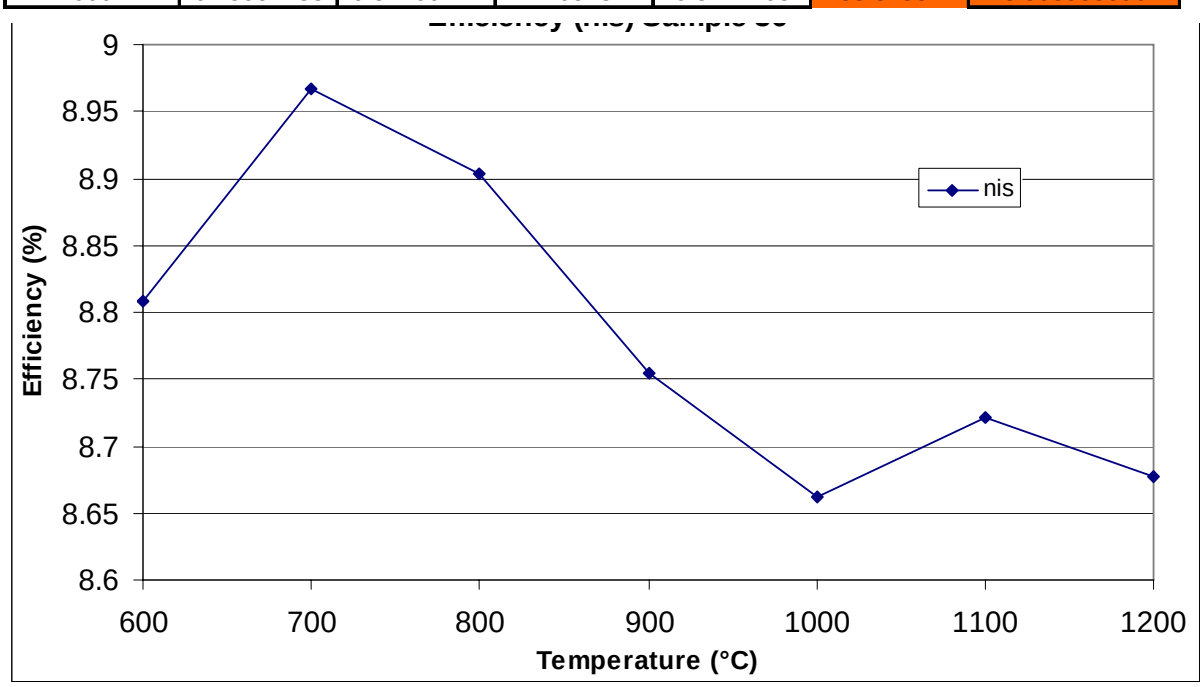

Figure 15. Efficiency η_{is} from ambient air experiments for sample 36.

As can be seen the efficiency does not change much over the temperature range indicating that sample properties do not change much over this temperature range.

The spray experiments were made using water nozzle Fulljet 1/8 GG 2 at 2.17 LPM and 3.14 LPM. In Figs. 16 and 17 the footprints for the nozzle at water flow rates 2 LPM and 3.4 LPM are shown respectively.

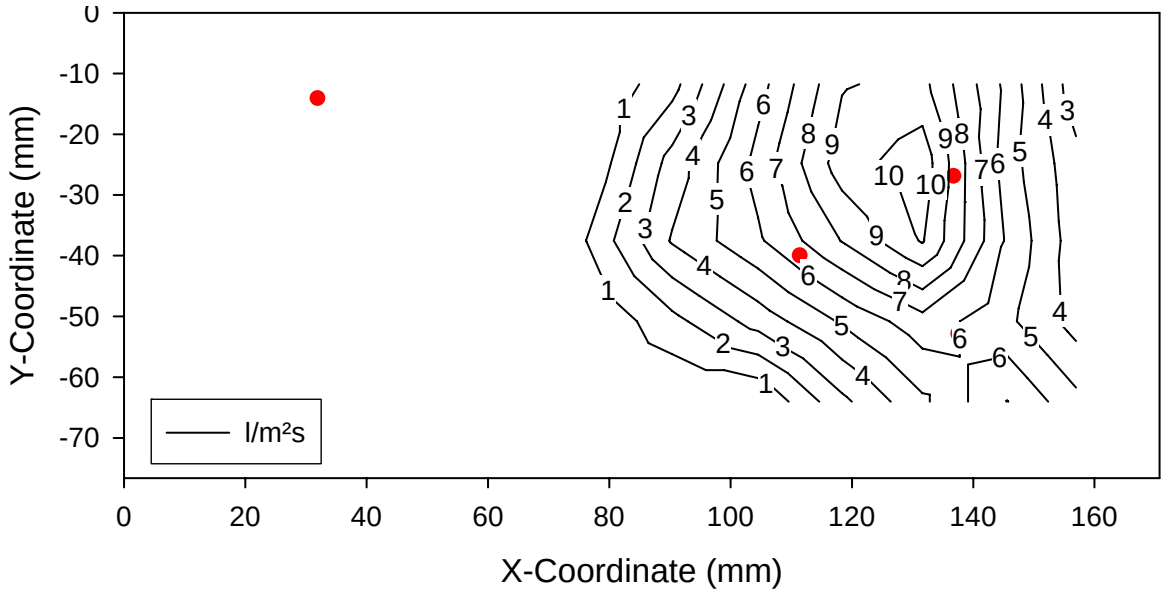

Figure 16. Footprint and thermocouple locations for unsteady state experiments for Fulljet 1/8 GG2 nozzle at 2 LPM water flow rate.

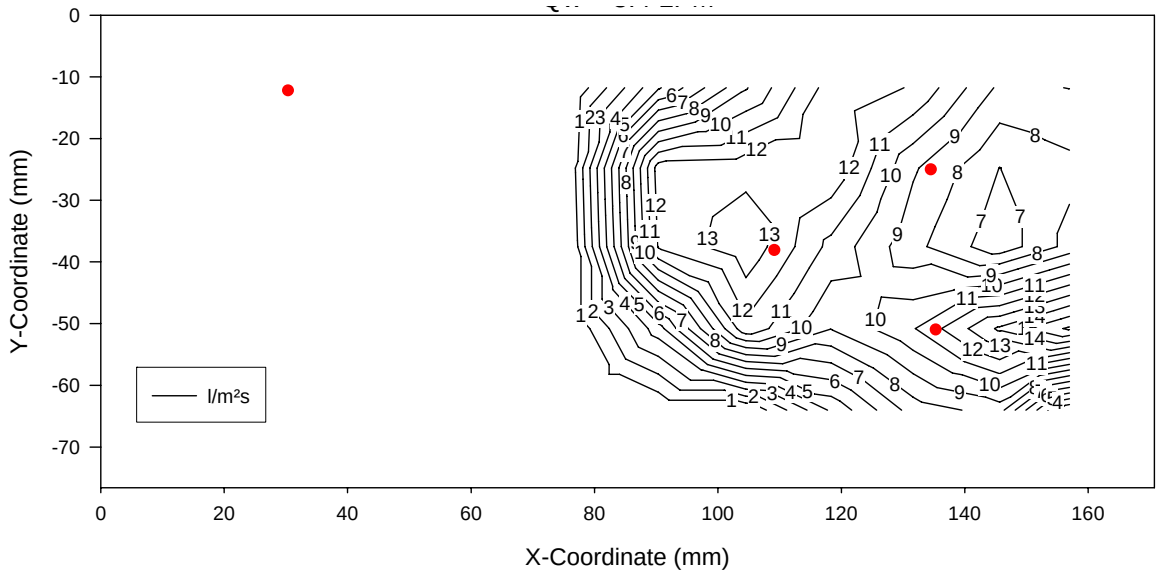

Figure 17. Footprint and thermocouple locations for unsteady state experiments for Fulljet 1/8 GG2 nozzle at 3.4 LPM water flow rate.

As with the efficiency calculations, first heat losses to ceramic and radiation are calculated using Eqs. 6 and 9. Results for sample 36 are shown in Table 3.

Table 3. Heat losses to air due to conduction and radiation for sample 36 in experiment with water flow rate 2.17 LPM.

Temperatura	P1a	P1b	P2	P3
1200	6.230264451	4.245838994	27.7885728	1.644282496
1100	4.700466205	3.203302663	25.39528672	1.486164621
1000	3.470812003	2.365310343	23.01136163	1.334652178
900	2.499210316	1.70317724	19.89856984	1.176303467
800	1.746751136	1.190386724	17.06744067	1.020893349
700	1.177705978	0.802590324	14.61438369	0.84826911
600	0.759527878	0.517607737	12.27804545	0.630966429

Table 4. Heat losses to air due to conduction and radiation for sample 36 in experiment with water flow rate 3.14 LPM.

Temperatura	P1a	P1b	P2	P3
1200	6.230264451	4.245838994	27.24122315	1.335057188
1100	4.700466205	3.203302663	25.1280268	1.297012166
1000	3.470812003	2.365310343	22.78954121	1.22244832
900	2.499210316	1.70317724	20.25808582	1.102344456
800	1.746751136	1.190386724	17.52785908	0.979590961
700	1.177705978	0.802590324	15.10551027	0.846451515
600	0.759527878	0.517607737	12.61402573	0.707899517

Because in the unsteady state experiments the radiation component of the heat extraction is in the results it is not subtracted like $P_{lateral}$, $P_{annular}$ and P_{back}.

In Table 4 heat losses are shown again and the averaged power over the time at the target temperature is calculated using Eq. 4b. These data is then used for calculate the heat extracted through the hole in the quartz using Eq. 12:

$$P_s = P_A \times \frac{\eta_{is}}{100} - P_{annular} - P_{lateral} - P_{back} \tag{12}$$

Where P_s is power extracted by the spray.

Table 4. Heat flux for sample 36 with water flow rate 2.17 LPM.

Calculo del flujo de calor en el experimento 1							
Calculo del flujo de calor usando potencias registradas en disco duro							
Temperatura	P2	P3	Pa	Eficiencia	Flujo de calor	Q (W/m2)	Q (MW/m2)
1200	27.7885728	1.644282496	977.8361127	8.677287392	51.17095543	1750946.83	1.750946832
1100	25.39528672	1.486164621	1034.796437	8.721822043	60.16834972	2058815.99	2.058815992
1000	23.01136163	1.334652178	1012.604265	8.661731586	60.99773928	2087195.7	2.087195705
900	19.89856984	1.176303467	1163.640232	8.755123098	79.10008415	2706614.34	2.706614341
800	17.06744067	1.020893349	1065.143617	8.903389169	75.55516066	2585315.6	2.585315598
700	14.61438369	0.84826911	937.560598	8.967143637	67.80716239	2320197.76	2.320197761
600	12.27804545	0.630966429	844.5054329	8.808935096	60.96531586	2086086.25	2.086086254

Table 5. Heat flux for sample 36 with water flow rate 3.14 LPM.

Calculo del flujo de calor usando potencias registradas en disco duro							
Temperatura	P2	P3	Pw	Eficiencia	Flujo de calor	ady state 3.14	Q (MW/m2) 3.14 LPM
1200	27.24122315	1.335057188	1572.605735	8.677287392	103.6373999	3546222.178	3.546222178
1100	25.1280268	1.297012166	1651.509796	8.721822043	114.4134038	3914951.075	3.914951075
1000	22.78954121	1.22244832	1501.644586	8.661731586	103.6911236	3548060.473	3.548060473
900	20.25808582	1.102344456	1294.459148	8.755123098	90.26788434	3088749.562	3.088749562
800	17.52785908	0.979590961	1094.483235	8.903389169	77.74826503	2660358.347	2.660358347
700	15.10551027	0.846451515	895.1139084	8.967143637	63.51159778	2173213.887	2.173213887
600	12.61402573	0.707899517	971.3815366	8.808935096	71.72883612	2454387.989	2.454387989

In Fig. 18 results from Tables 3 and 4 are compared with the corresponding transient experiments.

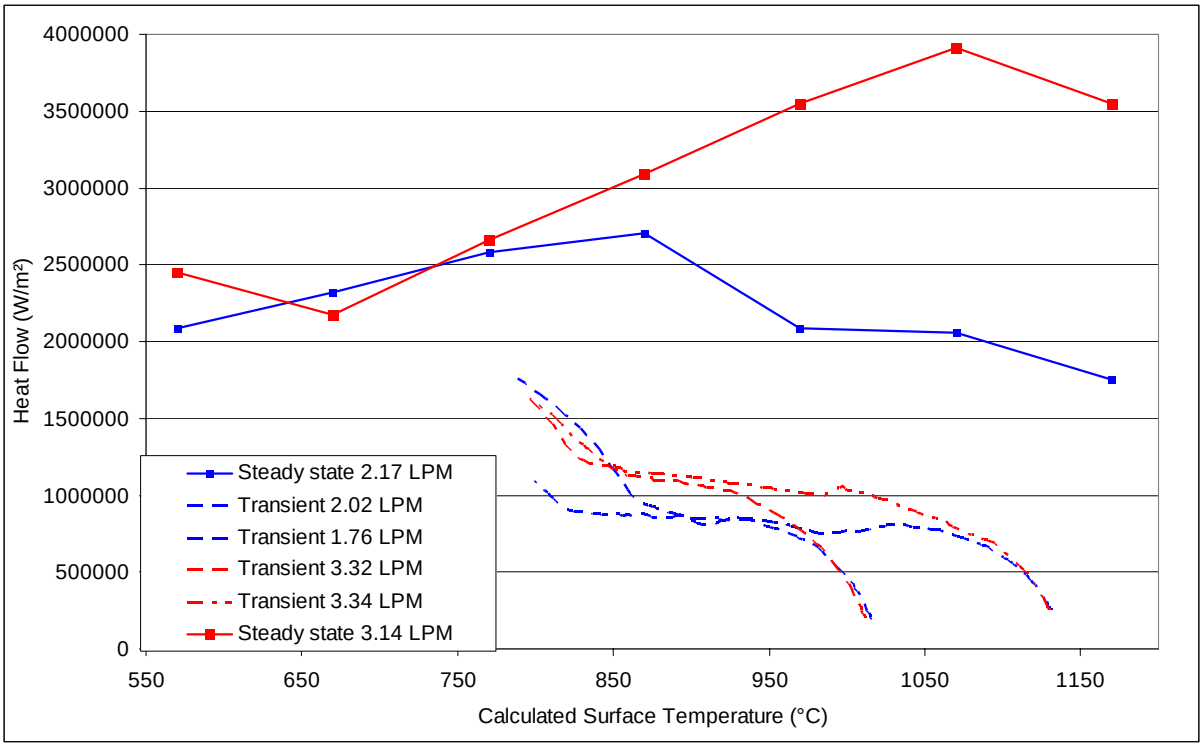

Figure 18. Comparison between transient and steady state heat flux for Fulljet 1/8 GG2 nozzle at flow rate ca. 2 and 3 LPM as a function of sample temperature (surface temp calculated by CONTA and a 2D model developed in CONDUCT).

The similar behavior in transient experiments show phenomenon reported by e.g. Mizikar [1] and Buyevich et. al [2] that at first the surface is hot and a non-wetting condition applies where the water just bounces of the sample surface without any major contribution to the total heat removal. The similarity also indicates strong time dependence due to layers build-up. Once the layers of water and vapor have been built, film-boiling regime is relatively insensitive to water flux, droplet size and surface temperature since water spray cannot exceed terminal momentum to penetrate the layers. In the case of steady state experiments it seems there is no such build-up but droplets are wetting the surface and figures indicate a dynamic Leidenfrost temperature effect where the hole in quartz seems to intercept the water from impinging the surface. This has to be confirmed with more experiments and by measuring water impact flux with a tube behind the quartz glass. As the temperature decreases the droplets start to penetrate the layers also in the transient experiments and at some point the heat flux values should be equal. It can be seen from Fig. 18 that curves get closer but not yet meet. There can be several reasons causing errors to both measurements: The annular heat loss is probably much more than just radiation and also other heat losses might be underestimated, measurement signals have errors in the steady state experiments. The errors possible in the transient experiments can be caused by thermocouples or the inverse model. The result look very promising and it is necessary to build a heat transfer model to estimate heat losses and match the know temperature points to be able to derive the surface temperature. The steady state experiment with flow rate 3.17 LPM was the second experiment with the sample 36 and it might cause lower efficiency due to oxidation and partial melting that is sometimes observed in the used samples.

3 Matching Mathematical Models of Heat Transfer Coefficients to Experiments

Usually mathematical heat transfer models use a mathematical model to estimate the heat transfer coefficient h in the secondary cooling zone. TEMPSIMU and CON1D use model developed by Nozaki and the equation is of the form:

$$h = a \times c \times Q^n \times c(T) \tag{13}$$

Where a and c are corrections factors, Q is the water flow rate, n a fitting parameter and c(T) a temperature dependent multiplier that is used to take into account the Leidenfrost effect. In Figs. 20 and 21 the experimental results are illustrated together with heat flux values derived from Eq. 13 using a*c = 0.3925 and n = 0.55 with and without the Leidenfrost effect. These values are the default values in CON1D. Used multipliers as a function of surface temperature are shown in the Fig. 19. The same Leidenfrost curve is used in the both cases.

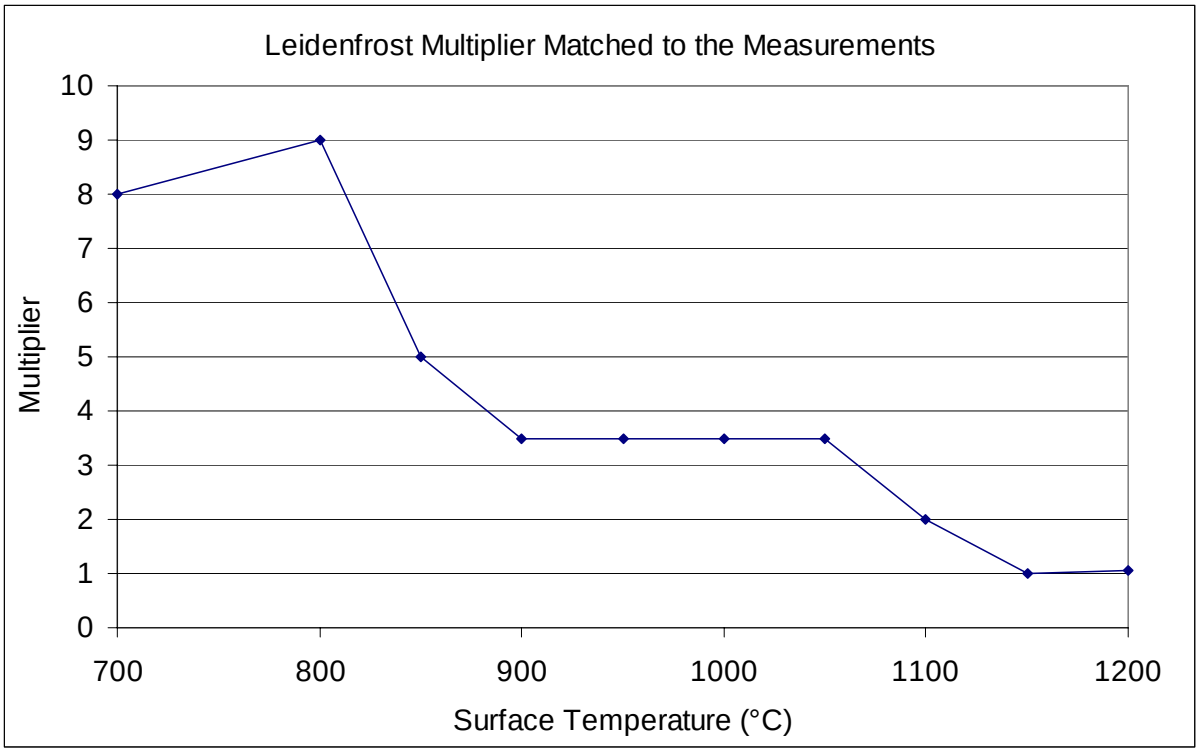

Figure 19.Leidenfrost multiplier in Eq. 13 as a function of surface temperature.

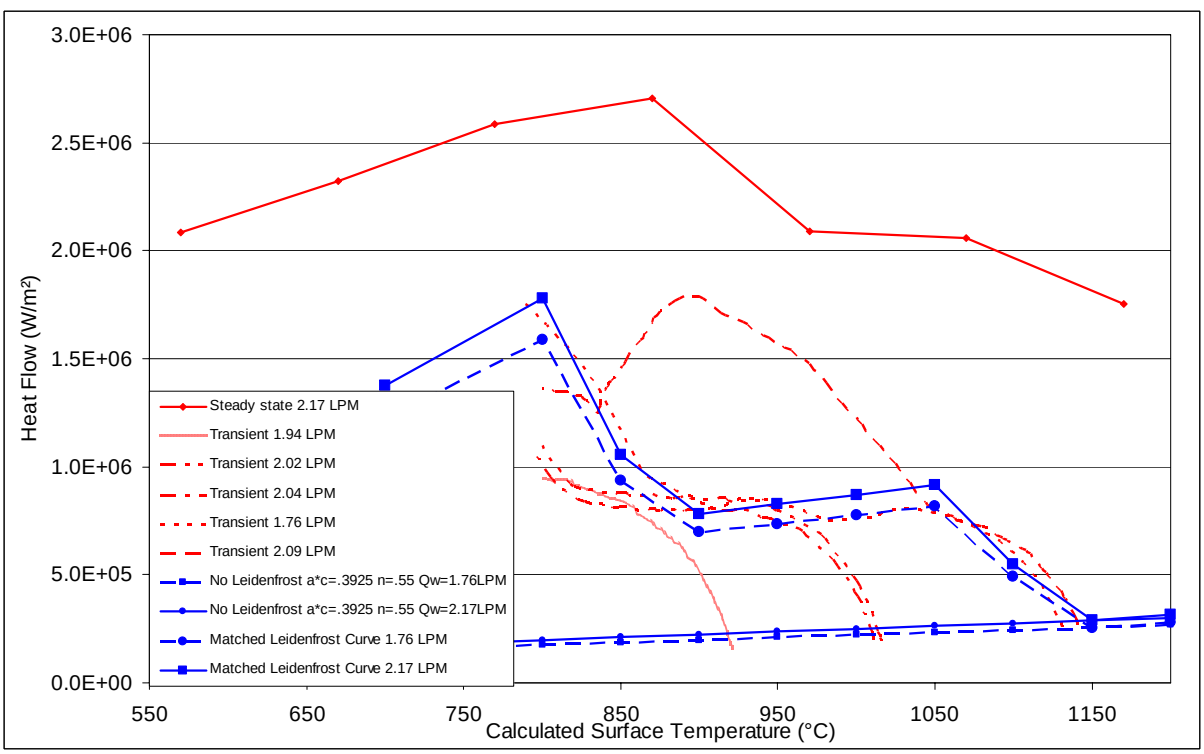

Figure 20. Heat flux values as a function of calculated surface temperature in the experiments with water flux ~2 LPM and calculated with Nozaki model with and without the Leidenfrost effect.

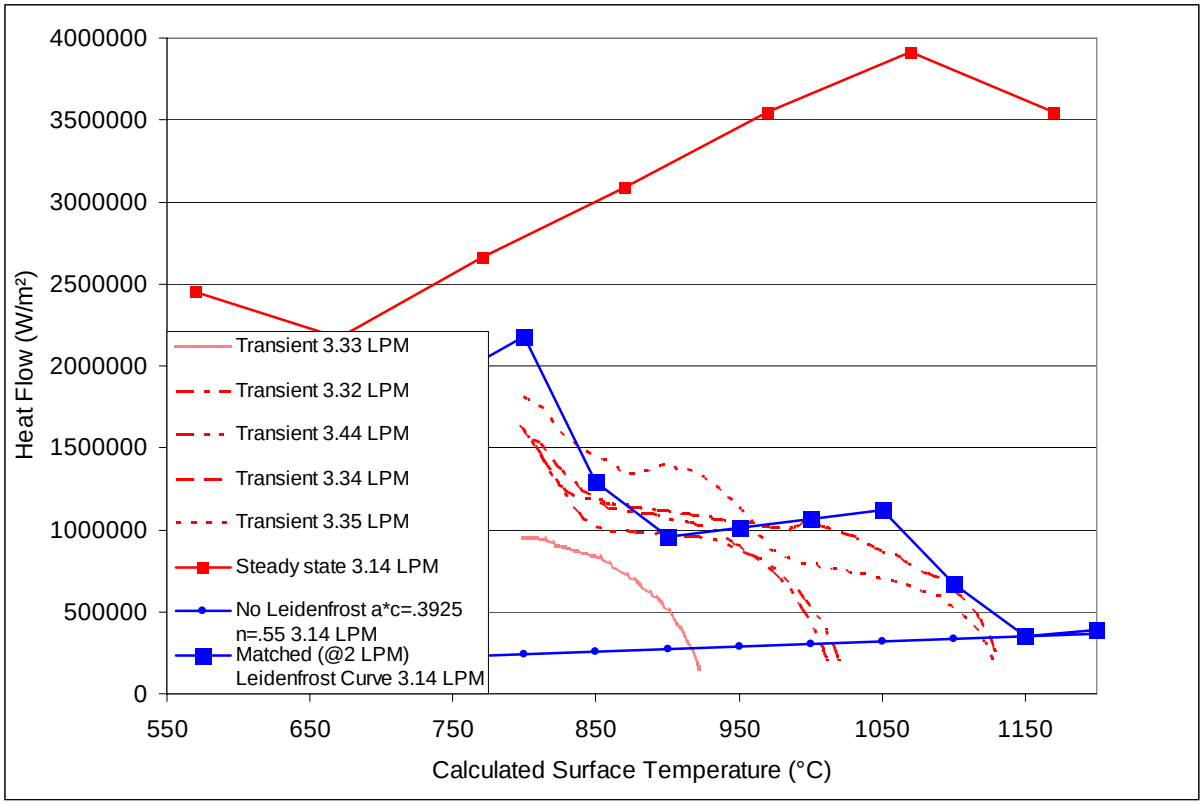

Figure 21. Heat flux values as a function of calculated surface temperature in the experiments with water flux ~3 LPM and calculated with Nozaki model with and without the Leidenfrost effect.

The amount of radiation heat losses compared to measured heat flux values can be seen in Fig 22.

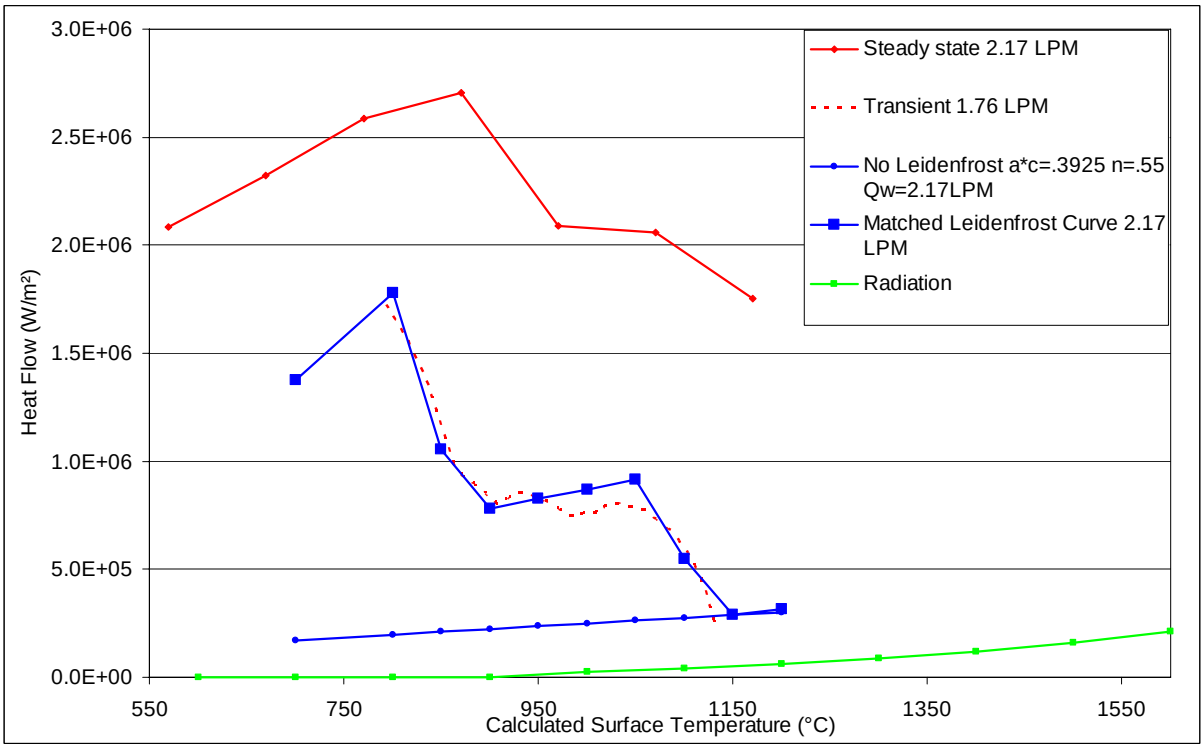

FUTURE WORK:

- Figures, tables and equations are not numbered
- Industrial validation
- Temperature vs. time for both transient and steady state measurements
- sensitivity analysis also for transient water spray
- Make conduct model to match our cases and develop the COMSOL model in 3D
- Conclusions

Air mist nozzle (suspected too high, owing to unmeasured, but expected lower power efficiency)

Note: max heat flux peak is still about 900 C, and Leidenfrost temp is 1200 C or higher.

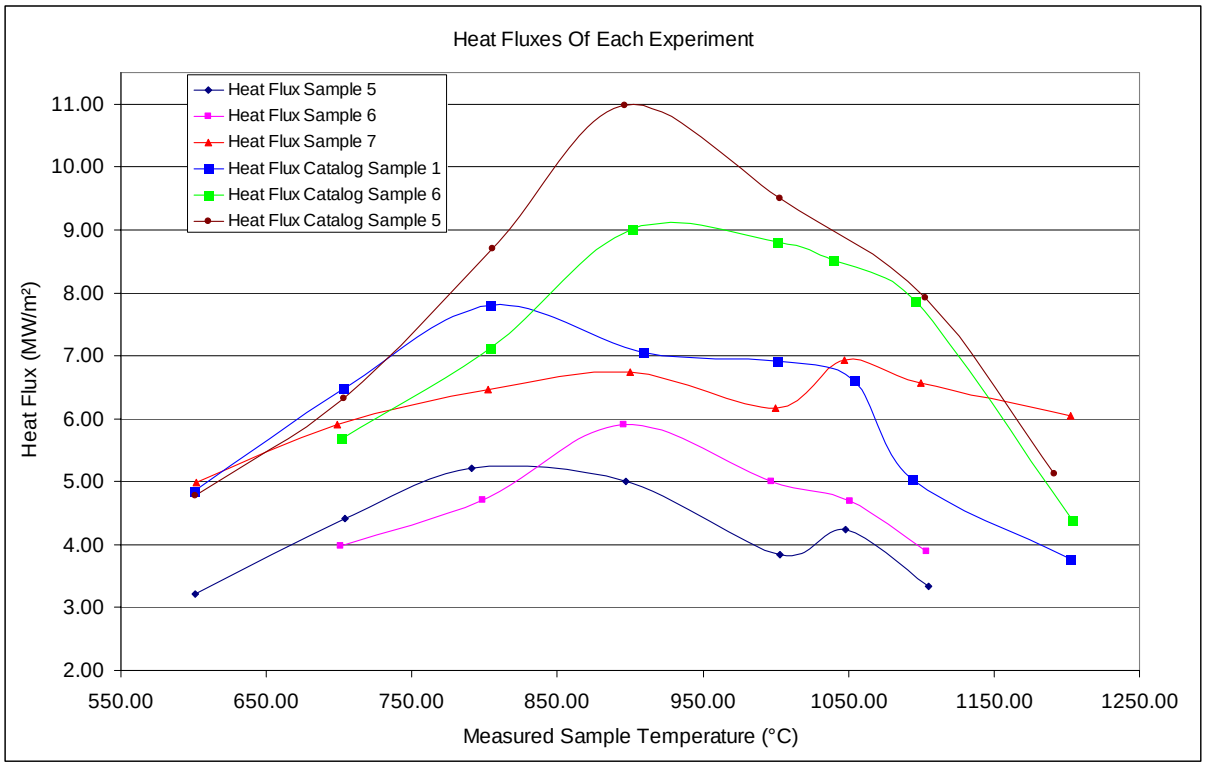

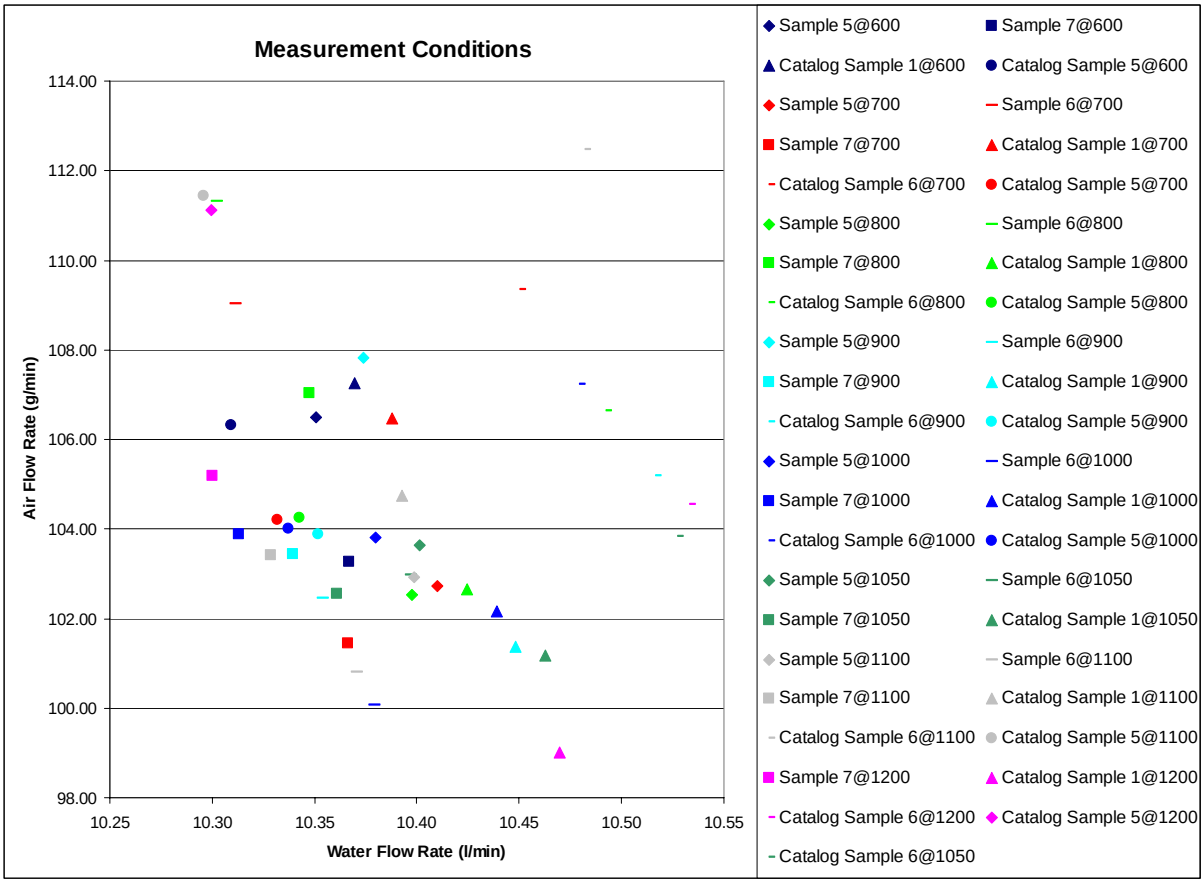

The peak heat flux temp is about 850C, (for 2 l/min) and increases to ~ 1050C (for 3 l/min). The higher peak is naturally expected for the higher water flow rate, as the droplets can better penetrate through the steam layers to reach the steel surface and boil. At the max, we expect a mixed water and steam layer on the surface, which causes efficient heat removal by unstable-film boiling, as droplets move around between the surface and the water and steam regions. Above this peak, the steam layer becomes dominant, and droplets have difficulty to penetrate it. Below this peak, the water layer dominates, and transport of the hot water within the water region occurs before it can boil as much.

The Leidenfrost temperature is very high (more than 1150 C), above our measurement range. This means that we are always working in a surface temperature regime, where the dynamic cooling involving Leidenfrost effects (steam layers, boiling, etc.) are always important!

Note that the transient measurements all have the same results at the beginning, meaning that initial heat flux is dominated by build-up of layers that varies with time. Minor surface temperature variations (even of a 100-200C) are not very important! Initially, droplets hit the surface and bounce off (due to the force of the gas expansion on forming steam layer at impact), so there is not much heat exchanged. This causes initial heat transfer rate to be slow, as there is too little water. The rate increases, as more water remains from previous droplets, so that new drops force other water to impinge, and a recirculating layer of boiling steam/water can develop. Eventually, (after 2-4s), the transient measurements should reach the steady-state values (but difficulties with both experimental methods makes the transient data still a little lower in the fig).

The steady-state measurements show much higher heat flux is ultimately obtained (after some time – 2-4 s has passed) for a given surface temperature.

At some very high surface temperature, (which depends on water and air flow rates), a stable steam film layer could form between the hot steel and the water layer, where the droplets hit and cannot

penetrate. This gives the lowest heat transfer rate (the Leidenfrost temperature). Increasing temperature eventually increases heat flux due to increased radiation.

The air-mist nozzle has higher heat transfer. It helps to get more use out of the existing water, but forcing droplets further through a water layer, and by mixing the existing water / steam layers. Thus, higher flux is found for a given water flux.

Implications for modelling: when leaving from beneath a roll, if the steel surface becomes “dry”, then the initial impact of the next water spray jet will take the steel through the transient heat-flux cycle (like the transient experiment) for 2-4s. Thus, the heat transfer will depend on casting speed for 2 reasons (changes the time / length of this region, and changes the surface temperature). If there is enough water for the region above the jet to remain wet at all times, then the steady-state heat flux values would likely dominate, and the transient heat flux is simply too small.

Implications of heat transfer mechanism: pressure behind the water droplets is very important, as their impact momentum determines how efficiently heat is transferred. Thus, pressure variations at the nozzle will greatly change the heat removal rate.

Thus, it is important to carefully monitor and control pressure.

References

1. CONTA manual

Appendix A.

Table 1. Sample catalog

	Before Measurement				After Measurement			
	Sample	Thickness, mm	Cone depth, mm	Diametrer, mm	Sample	Thickness, mm	Diametrer, mm	
acero inox 304	1	2.98	1.30	7.92	1.00	2.95	7.89	
acero inox 304	2	3.22	1.13	7.92	2.00	Melt		
acero inox 304	3	3.18	0.73	7.92	3.00	3.09	7.91	
acero inox 304	4	2.86	0.64	7.92	4.00	2.86	7.91	
acero inox 304	5	3.19	1.23	7.92	5.00	3.25	8.05	Partially melt
acero inox 304	6	3.46	1.00	7.92	6.00	3.69	8.29	Partially melt
acero inox 304	7	3.21	1.15	7.89				
acero inox 304	8	2.96	0.84	7.90				
acero inox 304	9	3.40	1.01	7.90				
acero inox 304	10	3.12	1.11	7.90				
acero inox 304	11	2.90	1.08	7.90				
acero inox 304	12	3.06	0.95	7.89				
acero inox 304	13	3.19	1.26	7.90				
acero inox 304	14	3.22	0.94	7.90		3.13	7.91	
acero inox 304	15	3.00	0.95	7.92				
acero inox 304	16	3.19	1.19	7.91				
acero inox 304	17	3.11	0.93	7.92				
acero inox 304	18	2.91	0.97	7.93				
acero inox 304	19	3.16	1.14	7.90				
acero inox 304	20	2.95	1.43	7.93				
acero inox 304	21	3.41	1.30	7.92				
acero inox 304	22	3.61	1.08	7.91				
acero inox 304	23	3.33	1.25	7.91				
acero inox 304	24	3.50	1.30	7.92				
acero inox 304	25	2.95	1.01	7.90				
acero inox 304	26	3.21	1.40	7.91				
acero inox 304	27	3.18	0.97	7.92				
acero inox 304	28	2.65	0.55	7.92	2.71		7.98	
acero inox 304	29	3.20	0.99	7.90	3.30		7.96	
acero inox 304	30	2.85	0.90	7.91				
acero inox 304	31	3.14	1.02	7.90				
acero inox 304	32	3.10	0.69	7.90	4.78		8.95	
acero inox 304	33	2.95	1.43	7.93		falló el termopar		
acero inox 304	34	3.11	1.49	7.91	3.04		7.89	
acero inox 304	35	3.31	1.57	7.91	3.27		7.71	
acero inox 304	36	3.35	0.59	7.91				
cobre	37	3.02	1.35	7.91		fundida		
acero inox 304	38	3.02	1.35	7.91				
acero inox 304	39	3.32	2.73	7.91				
acero inox 304	40	3.30	3.21	7.91				
acero inox 316	41	3.20	1.35	7.90				
acero inox 304	43	3.20	1.20	7.90				
acero inox 304	44	3.15	1.15	7.91				
acero inox 304	45	3.21	1.15	7.90				
	46							
	47							

Materials properties of materials:

Ceramic:

density 110 lbs/ft²

thermal expansion coeff 0.3 10e-6/°F

Thermal Conductivity 4 BTU in/Hr °F Ft²

Copper:

```
# -------------------------
# MATERIAL DATA : <CU-E>.SM
# -------------------------
#
# Pure Copper
#
# Equilibrium solidification !
#
# T[øC]  H[J/g] C[J/gK] K[W/Km] D[kg/m3]     V[Pas]  Event

104.62   31.18  0.3977  393.98  8896.72  6.000E+18  *
```

```
  99.62   29.19  0.3970  394.21  8899.09  6.000E+18  *
  94.62   27.21  0.3963  394.44  8901.45  6.000E+18  *
  89.62   25.23  0.3956  394.67  8903.81  6.000E+18  *
  84.62   23.25  0.3949  394.90  8906.17  6.000E+18  *
  79.62   21.28  0.3941  395.13  8908.53  6.000E+18  *
  74.62   19.31  0.3934  395.35  8910.88  6.000E+18  *
  69.62   17.35  0.3926  395.58  8913.23  6.000E+18  *
  64.62   15.39  0.3918  395.80  8915.58  6.000E+18  *
  59.62   13.43  0.3910  396.02  8917.92  6.000E+18  *
  54.62   11.48  0.3901  396.25  8920.26  6.000E+18  *
  49.62    9.53  0.3893  396.47  8922.60  6.000E+18  *
  44.62    7.58  0.3884  396.69  8924.93  6.000E+18  *
  39.62    5.65  0.3875  396.91  8927.26  6.000E+18  *
  34.62    3.71  0.3866  397.12  8929.59  6.000E+18  *
  29.62    1.78  0.3856  397.34  8931.91  6.000E+18  *
  25.00    0.00  0.3847  397.54  8934.06  6.000E+18  end
AISI 304L:
# THERMOPHYSICAL PROPERTIES for <AISI304>.RUN
#
# Stainless steel : Cr = 19.0000 wt%
#                   Ni = 10.0000 wt%
#                   Mn = 1.0000 wt%
#                   Si = 0.5000 wt%
#                   C  = 0.0700 wt%
#
# Cooling rate : 10.0 C/s below 1600 C
#
# Dendrite arm spacing :  27 um
#
#  T(C)   H(J/g) C(J/gK) K(W/Km) D(kg/m3)  Cont(%)    Alfa(1/K)    V(mPas)  Event

1600.00  1293.12  0.8401  84.586  6898.09   0.0000     0.00e-06  8.565e+00  *
1590.00  1284.73  0.8375  84.586  6905.71   0.0000    36.77e-06  8.655e+00  *
1580.00  1276.37  0.8348  84.586  6913.32   0.0000    36.74e-06  8.747e+00  *
1570.00  1268.03  0.8319  84.586  6920.93   0.0000    36.69e-06  8.843e+00  *
1560.00  1259.73  0.8290  84.586  6928.55   0.0000    36.65e-06  8.941e+00  *
1550.00  1251.45  0.8260  84.586  6936.16   0.0000    36.62e-06  9.043e+00  *
1540.00  1243.21  0.8229  84.586  6943.77   0.0000    36.57e-06  9.148e+00  *
1530.00  1234.99  0.8198  84.586  6951.39   0.0000    36.54e-06  9.256e+00  *
1520.00  1226.81  0.8165  84.586  6959.00   0.0000    36.49e-06  9.368e+00  *
1510.00  1218.66  0.8132  84.586  6966.61   0.0000    36.46e-06  9.484e+00  *
1500.00  1210.55  0.8098  84.586  6974.23   0.0000    36.42e-06  9.603e+00  *
1490.00  1202.47  0.8064  84.586  6981.84   0.0000    36.37e-06  9.726e+00  *
1480.00  1194.42  0.8029  84.586  6989.45   0.0000    36.34e-06  9.854e+00  *
1470.00  1186.41  0.7994  84.586  6997.07   0.0000    36.29e-06  9.985e+00  *
1451.89  1171.99  0.7928  84.586  7010.85   0.0000    36.29e-06  1.024e+01  LIQ_fer+
1450.67  1161.22  0.7902  81.757  7021.25   0.0494   405.25e-06  1.024e+01  *
1449.33  1150.15  0.7876  78.861  7031.88   0.0999   376.90e-06  1.024e+01  *
1447.92  1139.23  0.7849  76.026  7042.28   0.1492   349.19e-06  1.024e+01  *
1446.84  1131.38  0.7831  73.995  7049.72   0.1844   326.18e-06  1.024e+01  *
1445.73  1123.67  0.7812  72.012  7056.96   0.2188   307.50e-06  1.024e+01  *
1444.58  1116.11  0.7794  70.078  7064.02   0.2522   289.97e-06  1.024e+01  *
1443.39  1108.71  0.7776  68.193  7070.90   0.2847   273.14e-06  1.024e+01  *
```

1442.17	1101.44	0.7759	66.356	7077.58	0.3163	256.67e-06	1.024e+01	*
1440.90	1094.33	0.7742	64.567	7084.08	0.3470	241.36e-06	1.025e+01	*
1439.59	1087.36	0.7725	62.827	7090.39	0.3767	226.60e-06	1.025e+01	*
1438.23	1080.54	0.7709	61.135	7096.51	0.4056	212.45e-06	1.025e+01	*
1436.83	1073.86	0.7693	59.492	7102.45	0.4336	199.22e-06	1.026e+01	*
1435.39	1067.32	0.7678	57.897	7108.21	0.4607	186.30e-06	1.026e+01	*
1433.89	1060.93	0.7663	56.350	7113.77	0.4870	174.17e-06	1.027e+01	*
1432.33	1054.67	0.7648	54.852	7119.16	0.5123	162.53e-06	1.028e+01	*
1430.72	1048.55	0.7633	53.402	7124.37	0.5368	151.44e-06	1.029e+01	*
1429.06	1042.57	0.7619	52.001	7129.40	0.5605	140.95e-06	1.030e+01	*
1427.32	1036.71	0.7605	50.647	7134.25	0.5833	130.99e-06	1.031e+01	*
1425.52	1030.99	0.7592	49.342	7138.93	0.6053	121.49e-06	1.033e+01	*
1423.65	1025.40	0.7578	48.086	7143.44	0.6264	112.51e-06	1.034e+01	*
1421.71	1019.93	0.7565	46.878	7147.77	0.6468	104.01e-06	1.036e+01	*
1420.71	1017.24	0.7559	46.292	7149.88	0.6567	98.03e-06	1.038e+01	*
1419.68	1014.59	0.7553	45.718	7151.95	0.6664	94.05e-06	1.039e+01	*
1419.61	1014.22	0.7552	45.678	7151.83	0.6658	94.05e-06	1.038e+01	aus+
1418.51	1011.33	0.7542	45.139	7155.75	0.6842	167.05e-06	1.043e+01	*
1416.53	1004.96	0.7520	44.025	7163.96	0.7227	192.44e-06	1.053e+01	zst
1415.50	1001.81	0.7509	43.487	7168.07	0.7420	187.26e-06	1.058e+01	*
1414.46	998.70	0.7498	42.964	7172.14	0.7610	181.24e-06	1.063e+01	*
1413.39	995.62	0.7487	42.453	7176.18	0.7799	175.08e-06	1.068e+01	*
1412.29	992.57	0.7476	41.956	7180.17	0.7986	169.15e-06	1.074e+01	*
1411.17	989.56	0.7465	41.472	7184.13	0.8171	163.22e-06	1.079e+01	*
1410.01	986.58	0.7455	41.001	7188.03	0.8354	157.37e-06	1.085e+01	*
1408.84	983.63	0.7444	40.543	7191.90	0.8535	152.07e-06	1.091e+01	*
1407.63	980.72	0.7434	40.099	7195.72	0.8713	146.56e-06	1.097e+01	*
1406.39	977.84	0.7424	39.667	7199.49	0.8890	141.51e-06	1.104e+01	*
1405.13	974.99	0.7414	39.249	7203.22	0.9064	136.48e-06	1.110e+01	*
1403.84	972.18	0.7404	38.845	7206.89	0.9235	131.57e-06	1.117e+01	*
1402.52	969.41	0.7394	38.453	7210.51	0.9404	127.16e-06	1.124e+01	*
1401.18	966.67	0.7384	38.074	7214.08	0.9570	122.58e-06	1.131e+01	*
1399.81	963.97	0.7375	37.709	7217.58	0.9734	118.34e-06	1.138e+01	*
1398.42	961.32	0.7365	37.357	7221.03	0.9895	114.26e-06	1.146e+01	*
1397.00	958.70	0.7356	37.018	7224.41	1.0052	110.25e-06	1.153e+01	*
1395.57	956.12	0.7347	36.692	7227.72	1.0207	106.49e-06	1.161e+01	*
1394.11	953.59	0.7338	36.379	7230.96	1.0358	102.90e-06	1.169e+01	*
1392.65	951.11	0.7329	36.079	7234.13	1.0505	99.48e-06	1.177e+01	*
1391.17	948.69	0.7321	35.793	7237.22	1.0649	96.23e-06	1.185e+01	*
1389.68	946.31	0.7312	35.520	7240.22	1.0788	93.09e-06	1.193e+01	*
1388.20	944.00	0.7304	35.260	7243.13	1.0924	90.17e-06	1.202e+01	*
1386.72	941.76	0.7296	35.013	7245.94	1.1054	87.33e-06	1.210e+01	*
1385.25	939.58	0.7288	34.779	7248.65	1.1181	84.71e-06	1.218e+01	*
1383.79	937.48	0.7281	34.559	7251.25	1.1301	82.23e-06	1.226e+01	*
1382.36	935.46	0.7274	34.352	7253.73	1.1417	79.92e-06	1.234e+01	*
1380.97	933.52	0.7267	34.159	7256.10	1.1527	77.80e-06	1.242e+01	*
1379.61	931.68	0.7261	33.979	7258.33	1.1631	75.78e-06	1.250e+01	*
1378.31	929.94	0.7255	33.813	7260.43	1.1728	73.89e-06	1.257e+01	*
1377.06	928.32	0.7249	33.660	7262.39	1.1819	72.25e-06	1.264e+01	*
1375.89	926.81	0.7244	33.520	7264.19	1.1903	70.64e-06	1.271e+01	*
1374.80	925.42	0.7239	33.395	7265.84	1.1979	69.30e-06	1.277e+01	*
1372.90	923.05	0.7231	33.185	7268.64	1.2109	67.58e-06	1.288e+01	SOL
1371.00	920.45	0.7222	32.915	7271.65	1.2249	72.64e-06	5.900e+18	*

1370.00	919.60	0.7219	32.902	7272.62	1.2294	44.36e-06	5.900e+18	*
1369.00	918.77	0.7216	32.888	7273.51	1.2335	41.00e-06	5.900e+18	*
1368.00	917.94	0.7213	32.875	7274.39	1.2376	40.30e-06	5.900e+18	*
1367.00	917.11	0.7210	32.861	7275.26	1.2417	39.96e-06	5.900e+18	*
1366.00	916.29	0.7207	32.848	7276.13	1.2457	39.60e-06	5.900e+18	*
1365.00	915.47	0.7204	32.834	7276.99	1.2497	39.28e-06	5.900e+18	*
1364.00	914.65	0.7200	32.821	7277.84	1.2536	38.92e-06	5.900e+18	*
1363.00	913.84	0.7197	32.807	7278.68	1.2575	38.71e-06	5.900e+18	*
1362.00	913.02	0.7194	32.794	7279.52	1.2614	38.41e-06	5.900e+18	*
1361.00	912.21	0.7191	32.780	7280.35	1.2653	38.07e-06	5.900e+18	*
1360.00	911.40	0.7188	32.767	7281.18	1.2691	37.82e-06	5.900e+18	*
1359.00	910.59	0.7185	32.754	7282.00	1.2729	37.53e-06	5.900e+18	*
1358.00	909.78	0.7182	32.740	7282.81	1.2767	37.24e-06	5.900e+18	*
1357.00	908.98	0.7179	32.727	7283.62	1.2804	37.01e-06	5.900e+18	*
1356.00	908.18	0.7177	32.713	7284.42	1.2841	36.71e-06	5.900e+18	*
1355.00	907.38	0.7174	32.700	7285.22	1.2878	36.42e-06	5.900e+18	*
1354.00	906.58	0.7171	32.686	7286.01	1.2915	36.17e-06	5.900e+18	*
1353.00	905.78	0.7168	32.673	7286.79	1.2951	35.96e-06	5.900e+18	*
1352.00	904.99	0.7165	32.659	7287.58	1.2987	35.76e-06	5.900e+18	*
1351.00	904.19	0.7162	32.646	7288.35	1.3023	35.44e-06	5.900e+18	*
1350.00	903.40	0.7159	32.633	7289.12	1.3059	35.22e-06	5.900e+18	*
1349.00	902.61	0.7156	32.619	7289.89	1.3095	35.06e-06	5.900e+18	*
1348.00	901.82	0.7153	32.606	7290.65	1.3130	34.81e-06	5.900e+18	*
1347.00	901.04	0.7151	32.592	7291.41	1.3165	34.58e-06	5.900e+18	*
1346.00	900.25	0.7148	32.579	7292.16	1.3200	34.37e-06	5.900e+18	*
1345.00	899.47	0.7145	32.565	7292.90	1.3234	34.17e-06	5.900e+18	*
1344.00	898.69	0.7142	32.552	7293.65	1.3269	33.92e-06	5.900e+18	*
1343.00	897.90	0.7139	32.539	7294.38	1.3303	33.72e-06	5.900e+18	*
1342.00	897.12	0.7137	32.525	7295.12	1.3337	33.56e-06	5.900e+18	*
1341.00	896.35	0.7134	32.512	7295.85	1.3371	33.35e-06	5.900e+18	*
1340.00	895.57	0.7131	32.498	7296.57	1.3404	33.13e-06	5.900e+18	*
1339.00	894.80	0.7128	32.485	7297.30	1.3438	33.01e-06	5.900e+18	*
1338.00	894.02	0.7126	32.471	7298.01	1.3471	32.76e-06	5.900e+18	*
1337.00	893.25	0.7123	32.458	7298.73	1.3504	32.65e-06	5.900e+18	*
1336.00	892.48	0.7120	32.445	7299.44	1.3537	32.47e-06	5.900e+18	*
1335.00	891.71	0.7117	32.431	7300.15	1.3570	32.24e-06	5.900e+18	*
1334.00	890.94	0.7115	32.418	7300.85	1.3602	32.10e-06	5.900e+18	*
1333.00	890.17	0.7112	32.404	7301.55	1.3634	31.95e-06	5.900e+18	*
1332.00	889.41	0.7109	32.391	7302.24	1.3667	31.72e-06	5.900e+18	*
1331.00	888.64	0.7107	32.377	7302.94	1.3699	31.65e-06	5.900e+18	*
1330.00	887.88	0.7104	32.364	7303.63	1.3731	31.47e-06	5.900e+18	*
1329.00	887.12	0.7101	32.351	7304.31	1.3762	31.24e-06	5.900e+18	*
1328.00	886.35	0.7099	32.337	7305.00	1.3794	31.22e-06	5.900e+18	*
1327.00	885.59	0.7096	32.324	7305.67	1.3825	30.95e-06	5.900e+18	*
1326.00	884.84	0.7093	32.310	7306.35	1.3857	30.85e-06	5.900e+18	*
1325.00	884.08	0.7091	32.297	7307.02	1.3888	30.76e-06	5.900e+18	*
1324.00	883.32	0.7088	32.284	7307.69	1.3919	30.60e-06	5.900e+18	*
1323.00	882.56	0.7085	32.270	7308.36	1.3950	30.42e-06	5.900e+18	*
1322.00	881.81	0.7083	32.257	7309.03	1.3980	30.29e-06	5.900e+18	s50
1320.00	880.31	0.7078	32.230	7310.33	1.4041	29.85e-06	5.900e+18	*
1315.00	876.56	0.7065	32.163	7313.58	1.4191	29.63e-06	5.900e+18	*
1310.00	872.82	0.7052	32.096	7316.81	1.4340	29.41e-06	5.900e+18	*
1305.00	869.11	0.7039	32.029	7319.97	1.4486	28.81e-06	5.900e+18	*

1300.00	865.42	0.7027	31.962	7323.08	1.4630	28.27e-06	5.900e+18	*
1295.00	861.75	0.7014	31.896	7326.13	1.4771	27.76e-06	5.900e+18	*
1290.00	858.10	0.7002	31.829	7329.13	1.4909	27.33e-06	5.900e+18	*
1285.00	854.46	0.6990	31.762	7332.09	1.5046	26.91e-06	5.900e+18	*
1280.00	850.84	0.6978	31.695	7335.01	1.5181	26.55e-06	5.900e+18	*
1275.00	847.24	0.6966	31.629	7337.90	1.5314	26.22e-06	5.900e+18	*
1270.00	843.65	0.6954	31.562	7340.75	1.5445	25.89e-06	5.900e+18	*
1265.00	840.07	0.6943	31.495	7343.57	1.5575	25.62e-06	5.900e+18	*
1260.00	836.50	0.6931	31.429	7346.36	1.5704	25.35e-06	5.900e+18	*
1255.00	832.95	0.6919	31.362	7349.13	1.5831	25.11e-06	5.900e+18	*
1250.00	829.41	0.6908	31.296	7351.87	1.5958	24.87e-06	5.900e+18	*
1245.00	825.88	0.6896	31.229	7354.59	1.6083	24.68e-06	5.900e+18	*
1240.00	822.36	0.6885	31.163	7357.29	1.6207	24.47e-06	5.900e+18	*
1235.00	818.85	0.6874	31.096	7359.97	1.6331	24.29e-06	5.900e+18	*
1230.00	815.35	0.6862	31.030	7362.64	1.6454	24.13e-06	5.900e+18	*
1225.00	811.86	0.6851	30.964	7365.28	1.6575	23.95e-06	5.900e+18	*
1220.00	808.38	0.6840	30.897	7367.91	1.6696	23.81e-06	5.900e+18	*
1215.00	804.91	0.6829	30.831	7370.53	1.6817	23.66e-06	5.900e+18	*
1210.00	801.45	0.6818	30.765	7373.13	1.6936	23.53e-06	5.900e+18	*
1205.00	797.99	0.6807	30.699	7375.72	1.7055	23.41e-06	5.900e+18	*
1200.00	794.54	0.6796	30.632	7378.30	1.7174	23.28e-06	5.900e+18	*
1195.00	791.11	0.6785	30.566	7380.86	1.7291	23.18e-06	5.900e+18	*
1190.00	787.67	0.6774	30.500	7383.41	1.7409	23.05e-06	5.900e+18	*
1185.00	784.25	0.6763	30.434	7385.96	1.7525	22.95e-06	5.900e+18	*
1180.00	780.84	0.6752	30.368	7388.49	1.7642	22.86e-06	5.900e+18	*
1175.00	777.43	0.6742	30.302	7391.01	1.7758	22.76e-06	5.900e+18	*
1170.00	774.02	0.6731	30.236	7393.53	1.7873	22.67e-06	5.900e+18	*
1165.00	770.63	0.6720	30.170	7396.03	1.7988	22.59e-06	5.900e+18	*
1160.00	767.24	0.6709	30.104	7398.53	1.8102	22.50e-06	5.900e+18	*
1155.00	763.86	0.6699	30.038	7401.02	1.8217	22.43e-06	5.900e+18	*
1150.00	760.49	0.6688	29.973	7403.50	1.8330	22.35e-06	5.900e+18	*
1145.00	757.12	0.6678	29.907	7405.97	1.8444	22.28e-06	5.900e+18	*
1140.00	753.76	0.6667	29.841	7408.44	1.8557	22.22e-06	5.900e+18	*
1135.00	750.41	0.6657	29.775	7410.90	1.8670	22.13e-06	5.900e+18	*
1130.00	747.06	0.6646	29.710	7413.36	1.8782	22.08e-06	5.900e+18	*
1125.00	743.72	0.6636	29.644	7415.80	1.8894	22.01e-06	5.900e+18	*
1120.00	740.38	0.6626	29.578	7418.25	1.9006	21.95e-06	5.900e+18	*
1115.00	737.05	0.6615	29.513	7420.68	1.9118	21.90e-06	5.900e+18	*
1110.00	733.73	0.6605	29.447	7423.11	1.9229	21.83e-06	5.900e+18	*
1105.00	730.41	0.6595	29.382	7425.54	1.9340	21.79e-06	5.900e+18	*
1100.00	727.10	0.6584	29.316	7427.96	1.9451	21.73e-06	5.900e+18	*
1095.00	723.80	0.6574	29.251	7430.38	1.9561	21.69e-06	5.900e+18	*
1090.00	720.50	0.6564	29.185	7432.79	1.9672	21.63e-06	5.900e+18	*
1085.00	717.20	0.6554	29.120	7435.20	1.9782	21.58e-06	5.900e+18	*
1080.00	713.92	0.6544	29.054	7437.60	1.9891	21.54e-06	5.900e+18	*
1075.00	710.63	0.6534	28.989	7440.00	2.0001	21.48e-06	5.900e+18	*
1070.00	707.36	0.6523	28.924	7442.39	2.0110	21.45e-06	5.900e+18	*
1065.00	704.09	0.6513	28.859	7444.78	2.0220	21.40e-06	5.900e+18	*
1060.00	700.82	0.6503	28.793	7447.16	2.0329	21.36e-06	5.900e+18	*
1055.00	697.56	0.6493	28.728	7449.55	2.0437	21.32e-06	5.900e+18	*
1050.00	694.31	0.6483	28.663	7451.92	2.0546	21.28e-06	5.900e+18	*
1045.00	691.06	0.6473	28.598	7454.30	2.0654	21.24e-06	5.900e+18	*
1040.00	687.82	0.6464	28.533	7456.67	2.0762	21.20e-06	5.900e+18	*

1035.00	684.58	0.6454	28.468	7459.04	2.0870	21.16e-06	5.900e+18	*
1030.00	681.35	0.6444	28.403	7461.40	2.0978	21.12e-06	5.900e+18	*
1025.00	678.12	0.6434	28.338	7463.76	2.1086	21.09e-06	5.900e+18	*
1020.00	674.90	0.6424	28.273	7466.12	2.1193	21.05e-06	5.900e+18	*
1015.00	671.68	0.6414	28.208	7468.47	2.1301	21.02e-06	5.900e+18	*
1010.00	668.47	0.6405	28.143	7470.82	2.1408	20.99e-06	5.900e+18	*
1005.00	665.26	0.6395	28.078	7473.17	2.1515	20.96e-06	5.900e+18	*
1000.00	662.06	0.6385	28.013	7475.52	2.1622	20.91e-06	5.900e+18	*
995.00	658.86	0.6376	27.948	7477.86	2.1728	20.89e-06	5.900e+18	*
990.00	655.67	0.6366	27.884	7480.20	2.1835	20.86e-06	5.900e+18	*
985.00	652.49	0.6356	27.819	7482.53	2.1941	20.82e-06	5.900e+18	*
980.00	649.31	0.6347	27.754	7484.87	2.2047	20.79e-06	5.900e+18	*
975.00	646.13	0.6337	27.690	7487.20	2.2154	20.76e-06	5.900e+18	*
970.00	642.96	0.6328	27.625	7489.53	2.2260	20.74e-06	5.900e+18	*
965.00	639.80	0.6318	27.560	7491.85	2.2365	20.70e-06	5.900e+18	*
960.00	636.64	0.6309	27.496	7494.17	2.2471	20.67e-06	5.900e+18	*
955.00	633.48	0.6300	27.431	7496.49	2.2576	20.63e-06	5.900e+18	*
950.00	630.33	0.6290	27.367	7498.81	2.2682	20.61e-06	5.900e+18	*
945.00	627.18	0.6281	27.302	7501.13	2.2787	20.57e-06	5.900e+18	*
940.00	624.04	0.6271	27.238	7503.44	2.2892	20.55e-06	5.900e+18	*
935.00	620.91	0.6262	27.174	7505.75	2.2997	20.52e-06	5.900e+18	*
930.00	617.78	0.6253	27.109	7508.06	2.3102	20.49e-06	5.900e+18	*
925.00	614.65	0.6244	27.045	7510.36	2.3207	20.46e-06	5.900e+18	*
920.00	611.53	0.6234	26.981	7512.66	2.3311	20.43e-06	5.900e+18	*
915.00	608.41	0.6225	26.917	7514.96	2.3415	20.41e-06	5.900e+18	*
910.00	605.30	0.6216	26.852	7517.26	2.3520	20.38e-06	5.900e+18	*
905.00	602.19	0.6207	26.788	7519.55	2.3624	20.34e-06	5.900e+18	*
900.00	599.09	0.6198	26.724	7521.85	2.3728	20.32e-06	5.900e+18	*
895.00	595.99	0.6189	26.660	7524.13	2.3832	20.28e-06	5.900e+18	*
890.00	592.90	0.6180	26.596	7526.42	2.3935	20.25e-06	5.900e+18	*
885.00	589.81	0.6171	26.532	7528.70	2.4039	20.23e-06	5.900e+18	*
880.00	586.72	0.6162	26.468	7530.98	2.4142	20.19e-06	5.900e+18	*
875.00	583.65	0.6153	26.404	7533.26	2.4245	20.16e-06	5.900e+18	*
870.00	580.57	0.6144	26.340	7535.54	2.4349	20.12e-06	5.900e+18	*
865.00	577.50	0.6136	26.276	7537.81	2.4451	20.09e-06	5.900e+18	*
860.00	574.43	0.6127	26.212	7540.08	2.4554	20.07e-06	5.900e+18	*
855.00	571.37	0.6118	26.148	7542.34	2.4657	20.04e-06	5.900e+18	*
850.00	568.31	0.6110	26.085	7544.61	2.4759	20.00e-06	5.900e+18	*
845.00	565.26	0.6101	26.021	7546.87	2.4862	19.98e-06	5.900e+18	*
840.00	562.21	0.6092	25.957	7549.13	2.4964	19.94e-06	5.900e+18	*
835.00	559.17	0.6084	25.893	7551.38	2.5066	19.93e-06	5.900e+18	*
830.00	556.13	0.6075	25.830	7553.63	2.5168	19.88e-06	5.900e+18	*
825.00	553.09	0.6067	25.766	7555.88	2.5270	19.85e-06	5.900e+18	*
820.00	550.06	0.6059	25.702	7558.13	2.5371	19.81e-06	5.900e+18	*
815.00	547.03	0.6051	25.639	7560.37	2.5473	19.79e-06	5.900e+18	*
800.00	537.98	0.6026	25.448	7567.10	2.5777	19.76e-06	5.900e+18	endH
795.00	535.04	0.6018	25.385	7569.20	2.5872	18.53e-06	5.900e+18	*
790.00	532.03	0.6010	25.322	7571.44	2.5973	19.71e-06	5.900e+18	*
785.00	529.03	0.6002	25.258	7573.67	2.6074	19.68e-06	5.900e+18	*
780.00	526.03	0.5994	25.195	7575.91	2.6175	19.67e-06	5.900e+18	*
775.00	523.03	0.5987	25.132	7578.14	2.6276	19.66e-06	5.900e+18	*
770.00	520.04	0.5979	25.068	7580.37	2.6376	19.63e-06	5.900e+18	*
765.00	517.05	0.5971	25.005	7582.61	2.6477	19.63e-06	5.900e+18	*

760.00	514.07	0.5964	24.942	7584.84	2.6578	19.60e-06	5.900e+18	*
755.00	511.09	0.5956	24.879	7587.07	2.6678	19.59e-06	5.900e+18	*
750.00	508.11	0.5949	24.816	7589.29	2.6779	19.58e-06	5.900e+18	*
745.00	505.14	0.5942	24.753	7591.52	2.6879	19.56e-06	5.900e+18	*
740.00	502.17	0.5934	24.690	7593.75	2.6979	19.54e-06	5.900e+18	*
735.00	499.20	0.5927	24.627	7595.97	2.7080	19.53e-06	5.900e+18	*
730.00	496.24	0.5920	24.564	7598.19	2.7180	19.51e-06	5.900e+18	*
725.00	493.28	0.5914	24.501	7600.42	2.7280	19.50e-06	5.900e+18	*
720.00	490.33	0.5907	24.438	7602.64	2.7380	19.48e-06	5.900e+18	*
715.00	487.38	0.5900	24.375	7604.86	2.7480	19.46e-06	5.900e+18	*
710.00	484.43	0.5894	24.312	7607.08	2.7580	19.45e-06	5.900e+18	*
705.00	481.48	0.5888	24.249	7609.29	2.7680	19.43e-06	5.900e+18	*
700.00	478.54	0.5882	24.186	7611.51	2.7780	19.42e-06	5.900e+18	*
695.00	475.60	0.5876	24.124	7613.72	2.7879	19.40e-06	5.900e+18	*
690.00	472.66	0.5870	24.061	7615.94	2.7979	19.38e-06	5.900e+18	*
685.00	469.73	0.5865	23.998	7618.15	2.8078	19.37e-06	5.900e+18	*
680.00	466.80	0.5860	23.936	7620.36	2.8178	19.35e-06	5.900e+18	*
675.00	463.87	0.5855	23.873	7622.57	2.8277	19.33e-06	5.900e+18	*
670.00	460.94	0.5851	23.811	7624.78	2.8377	19.32e-06	5.900e+18	*
665.00	458.02	0.5846	23.748	7626.99	2.8476	19.30e-06	5.900e+18	*
660.00	455.10	0.5843	23.685	7629.20	2.8575	19.29e-06	5.900e+18	*
655.00	452.18	0.5839	23.623	7631.40	2.8674	19.27e-06	5.900e+18	*
650.00	449.26	0.5836	23.561	7633.61	2.8773	19.26e-06	5.900e+18	*
645.00	446.34	0.5834	23.498	7635.81	2.8872	19.24e-06	5.900e+18	*
642.44	444.85	0.5890	23.466	7636.94	2.8923	19.23e-06	5.900e+18	cur
640.00	443.41	0.5882	23.436	7638.01	2.8971	19.23e-06	5.900e+18	*
635.00	440.47	0.5868	23.373	7640.21	2.9070	19.20e-06	5.900e+18	*
630.00	437.54	0.5854	23.311	7642.41	2.9169	19.20e-06	5.900e+18	*
625.00	434.62	0.5840	23.249	7644.61	2.9267	19.17e-06	5.900e+18	*
620.00	431.70	0.5826	23.187	7646.81	2.9366	19.16e-06	5.900e+18	*
615.00	428.79	0.5812	23.124	7649.01	2.9464	19.15e-06	5.900e+18	*
610.00	425.89	0.5799	23.062	7651.20	2.9563	19.13e-06	5.900e+18	*
605.00	423.00	0.5786	23.000	7653.40	2.9661	19.12e-06	5.900e+18	*
600.00	420.11	0.5773	22.938	7655.59	2.9760	19.10e-06	5.900e+18	*
595.00	417.22	0.5760	22.876	7657.78	2.9858	19.09e-06	5.900e+18	*
590.00	414.35	0.5747	22.814	7659.97	2.9956	19.06e-06	5.900e+18	*
585.00	411.48	0.5735	22.752	7662.16	3.0054	19.05e-06	5.900e+18	*
580.00	408.61	0.5722	22.690	7664.35	3.0152	19.04e-06	5.900e+18	*
575.00	405.75	0.5710	22.628	7666.53	3.0250	19.02e-06	5.900e+18	*
570.00	402.90	0.5698	22.566	7668.72	3.0348	19.01e-06	5.900e+18	*
565.00	400.06	0.5686	22.504	7670.91	3.0446	18.99e-06	5.900e+18	*
560.00	397.22	0.5674	22.443	7673.09	3.0544	18.97e-06	5.900e+18	*
555.00	394.38	0.5663	22.381	7675.27	3.0641	18.96e-06	5.900e+18	*
550.00	391.55	0.5651	22.319	7677.45	3.0739	18.94e-06	5.900e+18	*
545.00	388.73	0.5640	22.257	7679.63	3.0837	18.93e-06	5.900e+18	*
540.00	385.91	0.5628	22.196	7681.81	3.0934	18.91e-06	5.900e+18	*
535.00	383.10	0.5617	22.134	7683.99	3.1032	18.90e-06	5.900e+18	*
530.00	380.30	0.5606	22.072	7686.17	3.1129	18.88e-06	5.900e+18	*
525.00	377.50	0.5595	22.011	7688.34	3.1226	18.87e-06	5.900e+18	*
520.00	374.70	0.5584	21.949	7690.51	3.1323	18.85e-06	5.900e+18	*
515.00	371.91	0.5573	21.888	7692.69	3.1420	18.84e-06	5.900e+18	*
510.00	369.13	0.5562	21.826	7694.86	3.1518	18.82e-06	5.900e+18	*
505.00	366.35	0.5551	21.765	7697.03	3.1614	18.80e-06	5.900e+18	*

500.00	363.58	0.5541	21.703	7699.20	3.1711	18.79e-06	5.900e+18	*
495.00	360.81	0.5530	21.642	7701.37	3.1808	18.77e-06	5.900e+18	*
490.00	358.05	0.5519	21.581	7703.54	3.1905	18.77e-06	5.900e+18	*
485.00	355.29	0.5509	21.519	7705.70	3.2002	18.73e-06	5.900e+18	*
480.00	352.54	0.5498	21.458	7707.87	3.2098	18.73e-06	5.900e+18	*
475.00	349.79	0.5488	21.397	7710.03	3.2195	18.71e-06	5.900e+18	*
470.00	347.05	0.5478	21.336	7712.19	3.2291	18.70e-06	5.900e+18	*
465.00	344.31	0.5467	21.274	7714.35	3.2388	18.68e-06	5.900e+18	*
460.00	341.58	0.5457	21.213	7716.51	3.2484	18.67e-06	5.900e+18	*
455.00	338.86	0.5447	21.152	7718.67	3.2580	18.64e-06	5.900e+18	*
450.00	336.14	0.5437	21.091	7720.83	3.2677	18.63e-06	5.900e+18	*
445.00	333.42	0.5427	21.030	7722.99	3.2773	18.63e-06	5.900e+18	*
440.00	330.71	0.5417	20.969	7725.14	3.2869	18.60e-06	5.900e+18	*
435.00	328.00	0.5407	20.908	7727.30	3.2965	18.59e-06	5.900e+18	*
430.00	325.30	0.5397	20.847	7729.45	3.3061	18.58e-06	5.900e+18	*
425.00	322.61	0.5387	20.786	7731.60	3.3157	18.56e-06	5.900e+18	*
420.00	319.92	0.5377	20.725	7733.75	3.3252	18.54e-06	5.900e+18	*
415.00	317.23	0.5367	20.664	7735.90	3.3348	18.53e-06	5.900e+18	*
410.00	314.55	0.5357	20.604	7738.05	3.3444	18.51e-06	5.900e+18	*
405.00	311.87	0.5347	20.543	7740.20	3.3539	18.50e-06	5.900e+18	*
400.00	309.20	0.5337	20.482	7742.34	3.3635	18.49e-06	5.900e+18	*
395.00	306.54	0.5328	20.421	7744.49	3.3730	18.47e-06	5.900e+18	*
390.00	303.87	0.5318	20.361	7746.63	3.3826	18.45e-06	5.900e+18	*
385.00	301.22	0.5308	20.300	7748.77	3.3921	18.44e-06	5.900e+18	*
380.00	298.57	0.5298	20.240	7750.92	3.4016	18.42e-06	5.900e+18	*
375.00	295.92	0.5289	20.179	7753.06	3.4111	18.41e-06	5.900e+18	*
370.00	293.28	0.5279	20.118	7755.19	3.4207	18.39e-06	5.900e+18	*
365.00	290.64	0.5269	20.058	7757.33	3.4302	18.37e-06	5.900e+18	*
360.00	288.01	0.5260	19.997	7759.47	3.4397	18.37e-06	5.900e+18	*
355.00	285.38	0.5250	19.937	7761.60	3.4491	18.34e-06	5.900e+18	*
350.00	282.76	0.5240	19.877	7763.74	3.4586	18.33e-06	5.900e+18	*
345.00	280.14	0.5231	19.816	7765.87	3.4681	18.32e-06	5.900e+18	*
340.00	277.53	0.5221	19.756	7768.00	3.4776	18.30e-06	5.900e+18	*
335.00	274.92	0.5212	19.696	7770.14	3.4870	18.29e-06	5.900e+18	*
330.00	272.32	0.5202	19.635	7772.27	3.4965	18.27e-06	5.900e+18	*
325.00	269.72	0.5192	19.575	7774.39	3.5059	18.25e-06	5.900e+18	*
320.00	267.12	0.5183	19.515	7776.52	3.5154	18.24e-06	5.900e+18	*
315.00	264.53	0.5173	19.455	7778.65	3.5248	18.22e-06	5.900e+18	*
310.00	261.95	0.5164	19.395	7780.77	3.5342	18.21e-06	5.900e+18	*
305.00	259.37	0.5154	19.335	7782.90	3.5436	18.19e-06	5.900e+18	*
300.00	256.80	0.5144	19.275	7785.02	3.5531	18.19e-06	5.900e+18	*
295.00	254.23	0.5135	19.215	7787.14	3.5625	18.16e-06	5.900e+18	*
290.00	251.66	0.5125	19.155	7789.26	3.5719	18.15e-06	5.900e+18	*
285.00	249.10	0.5116	19.095	7791.38	3.5813	18.14e-06	5.900e+18	*
280.00	246.55	0.5106	19.035	7793.50	3.5906	18.12e-06	5.900e+18	*
275.00	244.00	0.5096	18.975	7795.61	3.6000	18.11e-06	5.900e+18	*
270.00	241.45	0.5087	18.915	7797.73	3.6094	18.09e-06	5.900e+18	*
265.00	238.91	0.5077	18.855	7799.84	3.6188	18.08e-06	5.900e+18	*
260.00	236.37	0.5067	18.795	7801.96	3.6281	18.06e-06	5.900e+18	*
255.00	233.84	0.5057	18.736	7804.07	3.6375	18.05e-06	5.900e+18	*
250.00	231.32	0.5048	18.676	7806.18	3.6468	18.03e-06	5.900e+18	*
245.00	228.79	0.5038	18.616	7808.29	3.6561	18.02e-06	5.900e+18	*
240.00	226.28	0.5028	18.557	7810.40	3.6655	18.00e-06	5.900e+18	*

235.00	223.77	0.5018	18.497	7812.51	3.6748	17.99e-06	5.900e+18	*
230.00	221.26	0.5008	18.437	7814.61	3.6841	17.97e-06	5.900e+18	*
225.00	218.76	0.4998	18.378	7816.72	3.6934	17.96e-06	5.900e+18	*
220.00	216.26	0.4988	18.318	7818.82	3.7027	17.94e-06	5.900e+18	*
215.00	213.77	0.4978	18.259	7820.92	3.7120	17.92e-06	5.900e+18	*
210.00	211.28	0.4968	18.199	7823.03	3.7213	17.91e-06	5.900e+18	*
205.00	208.80	0.4958	18.140	7825.13	3.7306	17.90e-06	5.900e+18	*
200.00	206.33	0.4948	18.081	7827.23	3.7399	17.88e-06	5.900e+18	*
195.00	203.85	0.4938	18.021	7829.32	3.7491	17.87e-06	5.900e+18	*
190.00	201.39	0.4927	17.962	7831.42	3.7584	17.85e-06	5.900e+18	*
185.00	198.93	0.4917	17.903	7833.52	3.7676	17.84e-06	5.900e+18	*
180.00	196.47	0.4907	17.843	7835.61	3.7769	17.83e-06	5.900e+18	*
175.00	194.02	0.4896	17.784	7837.70	3.7861	17.81e-06	5.900e+18	*
170.00	191.57	0.4886	17.725	7839.80	3.7954	17.80e-06	5.900e+18	*
165.00	189.13	0.4875	17.666	7841.89	3.8046	17.77e-06	5.900e+18	*
160.00	186.70	0.4864	17.607	7843.98	3.8138	17.77e-06	5.900e+18	*
155.00	184.27	0.4853	17.548	7846.07	3.8230	17.74e-06	5.900e+18	*
150.00	181.85	0.4842	17.489	7848.15	3.8322	17.74e-06	5.900e+18	*
145.00	179.43	0.4831	17.430	7850.24	3.8414	17.72e-06	5.900e+18	*
140.00	177.01	0.4820	17.371	7852.33	3.8506	17.71e-06	5.900e+18	*
135.00	174.61	0.4809	17.312	7854.41	3.8598	17.69e-06	5.900e+18	*
130.00	172.21	0.4797	17.253	7856.49	3.8690	17.68e-06	5.900e+18	*
125.00	169.81	0.4786	17.194	7858.57	3.8782	17.66e-06	5.900e+18	*
120.00	167.42	0.4774	17.135	7860.65	3.8873	17.64e-06	5.900e+18	*
115.00	165.04	0.4762	17.076	7862.73	3.8965	17.64e-06	5.900e+18	*
110.00	162.66	0.4750	17.018	7864.81	3.9056	17.61e-06	5.900e+18	*
105.00	160.29	0.4738	16.959	7866.89	3.9148	17.61e-06	5.900e+18	*
100.00	157.92	0.4725	16.900	7868.96	3.9239	17.59e-06	5.900e+18	*
95.00	155.56	0.4712	16.842	7871.04	3.9331	17.58e-06	5.900e+18	*
90.00	153.21	0.4700	16.783	7873.11	3.9422	17.56e-06	5.900e+18	*
85.00	150.86	0.4687	16.724	7875.18	3.9513	17.54e-06	5.900e+18	*
80.00	148.52	0.4673	16.666	7877.26	3.9604	17.53e-06	5.900e+18	*
75.00	146.19	0.4660	16.607	7879.33	3.9695	17.52e-06	5.900e+18	*
70.00	143.86	0.4646	16.549	7881.39	3.9786	17.50e-06	5.900e+18	*
65.00	141.54	0.4632	16.490	7883.46	3.9877	17.49e-06	5.900e+18	*
60.00	139.23	0.4617	16.432	7885.53	3.9968	17.47e-06	5.900e+18	*
55.00	136.93	0.4602	16.374	7887.59	4.0059	17.46e-06	5.900e+18	*
50.00	134.63	0.4587	16.315	7889.66	4.0150	17.45e-06	5.900e+18	*
45.00	132.34	0.4572	16.257	7891.72	4.0240	17.43e-06	5.900e+18	*
40.00	130.06	0.4556	16.199	7893.78	4.0331	17.41e-06	5.900e+18	*
35.00	127.78	0.4539	16.140	7895.84	4.0421	17.40e-06	5.900e+18	*
30.00	125.52	0.4522	16.082	7897.90	4.0512	17.39e-06	5.900e+18	*
25.00	123.26	0.4505	16.024	7899.96	4.0602	17.37e-06	5.900e+18	endL